Neurovirulent murine coronavirus JHM.SD uses cellular zinc metalloproteases for virus entry and cell-cell fusion

Running title: Metalloproteases in murine coronavirus fusion

Judith M. Phillips[1#], Tom Gallagher[2], and Susan R. Weiss[1]

1) Department of Microbiology, Perelman School of Medicine, University of Pennsylvania, Philadelphia, PA, USA

2) Department of Microbiology and Immunology, Loyola University Medical Center, Maywood, Illinois, USA

Address correspondence to: Judith M. Phillips, jphil@upenn.edu

Abstract word count: 181

Importance word count: 147

Text word count: 6872

ABSTRACT

The coronavirus S protein requires cleavage by host cell proteases to mediate virus-cell and cell-cell fusion. Many strains of the murine coronavirus mouse hepatitis virus (MHV) have distinct, S-dependent organ and tissue tropisms despite using a common receptor, suggesting that they employ different cellular proteases for fusion. In support of this hypothesis, we found that inhibition of endosomal acidification only modestly decreased entry and overexpression of the cell surface protease TMPRSS2 greatly enhanced entry of the highly neurovirulent MHV strain JHM.SD relative to their effects on the reference strain A59. However, TMPRSS2 overexpression decreased MHV structural protein expression, release of infectious particles, and syncytia formation, and endogenous serine protease activity did not contribute greatly to infection. We therefore investigated the importance of other classes of cellular proteases and found that inhibition of MMP- and ADAM-family zinc metalloproteases markedly decreased both entry and cell-cell fusion. Suppression of virus by metalloprotease inhibition varied among tested cell lines and MHV S proteins, suggesting a role for metalloprotease use in strain-dependent tropism. We conclude that zinc metalloproteases must be considered potential contributors to coronavirus fusion.

IMPORTANCE

The family *Coronaviridae* includes viruses that cause two emerging diseases of humans, Severe Acute Respiratory Syndrome (SARS) Middle East Respiratory Syndrome (MERS), as well as a number of important animal pathogens. Because coronaviruses depend on host protease-mediated cleavage of their S proteins for entry, a

number of protease inhibitors have been proposed as antiviral agents. However, it is unclear which proteases mediate *in vivo* infection: for example, SARS-CoV infection of cultured cells depends on endosomal acid pH-dependent proteases rather than on the cell-surface acid pH-independent serine protease TMPRSS2, but Zhou et al. (Antiviral Res 116:76-84, 2015, doi:10.1016/j.antiviral.2015.01.011) found that a serine protease inhibitor was more protective than a cathepsin inhibitor in SARS-CoV-infected mice. This paper explores the contributions of endosomal acidification and various proteases to coronavirus infection and identifies an unexpected class of proteases, the matrix metalloproteinase and *A-D*isintegrin-*A*nd-*M*etalloprotease (ADAM) families, as potential targets for anti-coronavirus therapy.

INTRODUCTION

Entry of enveloped viruses requires viral surface proteins to attach to the cell surface and to undergo conformational changes that drive fusion of the viral and cellular membranes. Both steps can also involve host cell factors: attachment requires a cellular receptor recognized by the viral attachment protein, and fusion may require cellular processes such as endocytosis and endosomal acidification and/or cleavage of viral surface proteins by host cell proteases. While receptor availability is a major determinant of viral species and tissue tropism, other host fusion factors can also contribute: for example, low-pathogenicity strains of avian influenza virus require cleavage of the fusion protein HA by trypsin-like proteases, confining the virus to the digestive and respiratory tracts where such enzymes are available, whereas high-pathogenicity strains have HA sequences that can be cleaved by ubiquitously expressed proteases and thus cause systemic infection (reviewed in (1)). Host cell fusion factors are therefore potential targets for antiviral therapy.

The emergence of severe acute respiratory syndrome (SARS) and Middle East respiratory syndrome (MERS) as human diseases has prompted interest in anti-coronavirus strategies, including inhibition of host cell proteases involved in coronavirus fusion (2). Coronaviruses rely on a single spike (S) protein for attachment and fusion, and fusion requires proteolytic cleavage of S by host proteases during the viral replication cycle (reviewed in (3)). S comprises an N-terminal S1 portion, containing the receptor-binding domain (RBD), and a C-terminal S2 portion, containing the fusion machinery. In some coronavirus species, S is cleaved at the S1/S2 boundary, typically by a furin-like protease in the producing cell during virus assembly and/or egress; S1 and S2 remain

76 associated via non-covalent interactions (3). In murine coronavirus, furin cleavage at
77 S1/S2 is not required for infection but appears to be necessary for cell-cell fusion, as
78 mutation of the site (4-6) or pharmacologic inhibition of furin-like proteases (7) affects
79 syncytia formation; insertion of a furin cleavage site at S1/S2 also enhances cell-cell
80 fusion by SARS coronavirus (8). Fusion is also thought to require an additional
81 proteolytic cleavage within S2 at the N-terminus of the fusion peptide, resulting in a new
82 C-terminal fragment sometimes called S2′ (reviewed in (3) and (9)). Members of at least
83 four groups of proteases have been implicated in the S2′ cleavage: cathepsins B and L,
84 which are acid-dependent endosomal cysteine proteases; *t*rans*m*embrane *p*rotease, *s*erine
85 (TMPRSS)-family proteases, especially TMPRSS2, which are acid-independent serine
86 proteases generally found at the cell surface; elastases, which are common serine-family
87 proteases in lung tissue; and furin-like pro-protein convertases. Inhibitors of cathepsins B
88 and L block entry by many coronaviruses, including SARS-CoV (10, 11) and MERS-
89 CoV (12, 13), feline coronavirus (14), and the mouse hepatitis virus (MHV) strain MHV-
90 2 (4). The role of TMPRSS2 is less clear. It appears to promote infection by SARS-CoV
91 (15-17), MERS-CoV (12, 13), the human respiratory coronavirus NL63 (18), and clinical
92 isolates of the human respiratory coronavirus 229E (19), especially when endosomal
93 acidification or cathepsin activity is inhibited, and also increases infection and virus
94 release by otherwise trypsin-dependent strains of porcine epidemic diarrhea virus
95 (PEDV) (20). TMPRSS2 is thought to cleave and thus activate some influenza HA
96 proteins (21, 22), and it may increase SARS-CoV entry by cleaving the S protein or by
97 enhancing virus particle uptake via specific cleavage of the SARS-CoV receptor ACE2
98 (16, 23). A number of extracellular proteases, including elastase, enhance SARS-CoV

infection (24), and a putative elastase site has been identified within S2 (25). The fourth protease, furin, has a cleavage substrate motif that is found at the N-terminus of the putative fusion peptide in MERS-CoV (26, 27) and the embryo-adapted Beaudette strain of the avian coronavirus infectious bronchitis virus (IBV) (8). Furin does appear to cleave at this site, and furin activity enhances MERS-CoV infection (27). Finally, a fifth category of proteases plays a controversial role in SARS-CoV entry: the metalloprotease ADAM17/TACE has been reported to enhance SARS-CoV uptake by cleaving ACE2 (28, 29), although other authors have disagreed (23, 30). Inhibition of proteases implicated in viral fusion is now under investigation as an anti-coronavirus strategy, with promising results: camostat, an inhibitor of serine proteases including TMPRSS2, was recently shown to reduce mortality in a mouse model of SARS-CoV infection, whereas a cathepsin inhibitor that decreased SARS-CoV entry *in vitro* had minimal effect in the infected mice (2). The effect of TMPRSS2 seems particularly context-specific: clinical but not culture-adapted strains of 229E are TMPRSS2-dependent (19), and MERS-CoV requires TMPRSS2 for infection of some respiratory cells but not other cell lines (31). The diversity of proteases involved in coronavirus entry may thus complicate the search for effective treatments, as the protease dependence of a particular coronavirus may vary among target cells.

If the specific protease dependence of coronavirus fusion depends on the cell type being infected, as the *in vivo* data suggest, then coronaviruses may have evolved to use different proteases to infect different sites. This would make protease use a potential determinant of coronavirus organ and tissue tropism, as for avian influenza. We sought to explore this possibility using the murine coronavirus MHV as a model. MHV is useful

for studying the contribution of host fusion factors to coronavirus tropism because infection of the laboratory mouse, a natural host, has identified a number of strains that appear to use the same receptor, CEACAM1a, but exhibit diverse cell, tissue, and organ specificities. We chose to focus on the brain-adapted strain JHM.SD (formerly named MHV4; GenBank: FJ647219.1) because its extreme neurovirulence is largely S protein-dependent (32, 33) and because the JHM.SD spike also displays an unusual cell-to-cell spread phenotype that may indicate exceptional susceptibility to S2′ cleavage: JHM.SD forms syncytia when infected cells are overlaid on non-permissive (i.e., receptor-lacking) cells, a process known as "receptor-independent spread" (34). Furthermore, CEACAM1a is poorly expressed in the brain and almost absent on neurons, yet viruses bearing the JHM.SD spike spread extensively in infected brains and in neurons from wild-type or *Ceacam1a*$^{-/-}$ mice (35, 36). These properties led us to speculate that the JHM.SD spike might have adapted to the low level of receptor in the brain by becoming more sensitive to cleavage by an available protease. The CEACAM1a-independent cell-to-cell spread phenotype and the insensitivity of JHM.SD infection to endosomotropic weak bases (37) strongly suggested the involvement of a cell-surface protease such as TMPRSS2. We therefore hypothesized that JHM.SD infection is more sensitive than other MHV strains to a cell-surface protease and that this difference is responsible for the neurotropism of the JHM.SD spike.

In this study, we examined the dependence of JHM.SD infection on endosomal acidification (and thereby acid-dependent endosomal proteases) and the neutral cell surface protease TMPRSS2 and found that JHM.SD was less sensitive to inhibition of endosomal acidification but more sensitive to TMPRSS2 expression than the moderately

neurovirulent reference strain A59. However, inhibitor studies revealed at best a minor role for surface serine proteases in MHV virus-cell and cell-cell fusion; instead, an unidentified cell-surface metalloprotease appears to mediate these activities in the cell lines examined. These results suggest that sensitivity to a metalloprotease available in the brain may underlie the tropism of JHM.SD.

MATERIALS AND METHODS

Viruses and Cells. Recombinant MHV strains rJHM.SD-fluc and rA59-fluc were generated by targeted RNA recombination according to the methods developed by Kuo et al (38) and Masters and Rottier (39). The firefly luciferase gene was included between the viral E and M genes, as originally done by de Haan et al. (40). The luciferase-expressing viruses were grown in DBT cells, and stocks were expanded from single luciferase-positive plaques. Recombinant MHV strains icJHM.SD (41), rA59 (32), and rA59/S_{MHV-2} (42) and enhanced green fluorescent protein (EGFP)-expressing strains rA59/$S_{JHM.SD}$-EGFP, rA59-EGFP (43), and rA59/S_{MHV-2}-EGFP (4) were grown in 17Cl1 cells. All viruses were titered on L2 cells as previously described (44), and all multiplicity of infection (MOI) calculations were based on L2 cell titers. Viruses were diluted in Dulbecco's modified Eagle's medium (DMEM) with 2% fetal bovine serum (FBS) for inoculation unless otherwise indicated.

Human embryonic kidney (HEK) 293T cells were maintained in DMEM (Gibco 11965-084) with 100 U/mL penicillin and 100 µg/mL streptomycin and 10% fetal bovine serum (FBS); HEK-293β5 cells (human embryonic kidney cells overexpressing the human β5 integrin subunit) were maintained in the same medium with 100 µg/mL G418.

168 DBT cells were maintained in DMEM with 100 U/mL penicillin and 100 µg/mL
169 streptomycin, 5% FBS, and 10% tryptose phosphate broth. L2 and 17Cl1 cells were
170 maintained in reconstituted DMEM (Gibco 12100-061) with 0.37% sodium bicarbonate,
171 10 mM HEPES, 2 mM glutamine, 100 U/mL penicillin and 100 µg/mL streptomycin, and
172 10% FBS.
173
174 *Inhibitors.* Bafilomycin A1 (Calbiochem 96000), camostat (Sigma SML0057), E64
175 (Sigma E3132), pepstatin A (Roche Boehringer Mannheim 11359053001), batimastat
176 (Sigma SML0041), and furin inhibitor I (Calbiochem 344930) were dissolved in dimethyl
177 sulfoxide (DMSO) at 200× (bafilomycin A) or 100× (protease inhibitors) the highest final
178 concentration indicated for the entry and L2 cell spread assays and at 2000× the final
179 concentration for the HEK-293β5 cell spread assays. The inhibitors were stored in
180 working aliquots at −20°C and added to the medium immediately before use.
181
182 *Plasmids and transfection.* pCAGGS-h*TMPRSS2*-FLAG (wt) and pCAGGS-h*TMPRSS2*-
183 S441A-FLAG are described in (16). pCAGGS-m*Ceacam1a*-4L was made by inserting a
184 PCR product amplified from BgpD (Genbank X67279.1) into the EcoRI and KpnI sites
185 of pCAGGS-MCS. pTK-*mCeacam1a*-4L was made by inserting a PCR product amplified
186 from BgpD into the Not I backbone of pTKbeta (ATCC® 77178™). The nucleotide
187 sequences of all PCR-derived segments were confirmed by sequencing. The day before
188 transfection, HEK-293T cells were seeded in 6-well plates at 1×10^6 cells/well and HEK-
189 293β5 cells were seeded in 24-well plates at 1.3×10^5 cells/well. For transfection, 3 µg
190 plasmid (comprising 1200 ng of pCAGGS-m*Ceacam1a*-4L or pTK-m*Ceacam1a*-4L, up

191 to 600 ng pCAGGS-h*TMPRSS2*-FLAG, and the balance as empty vector pCAGGS-
192 MCS) was diluted into 200 µL of OptiMEM and then 9 ug of polyethylenimine
193 (Polysciences, Inc. 23966 at 1 µg/µL, pH 7.0; 3:1 w/w ratio) was added. The reactions
194 were incubated at room temperature for 15 min and then added to the cells (150 µL/well
195 for 6-well plates and 30 µL/well for 24-well plates); for consistency, the amounts of
196 pCAGGS-h*TMPRSS2*-FLAG are always shown as the equivalent amount for a 6-well
197 plate well. Transfected HEK-293T cells were re-seeded into smaller wells 1 day post-
198 transfection (dpt) as described in the individual experiments.
199 *Entry and viability assays.* L2 cells (1×10^5 cells/well), 17Cl1 cells (5×10^4 cells/well),
200 and DBT cells (5×10^4 cells/well) were seeded in tissue culture-treated white 96-well
201 plates 1 day before infection. In the luciferase reporter experiments (Figures 1, 2, 4, and
202 5), the cells were pretreated for 3 h with protease inhibitors or DMSO and/or 1 h with
203 bafilomycin A or additional DMSO (pre-infection treatment); the post-infection treatment
204 cells (Figures 1 and 4) were not disturbed. Virus was diluted to achieve the indicated
205 MOI in 50 µL/well, and inhibitors were added to the inoculum at the indicated
206 concentrations (pre-infection treatment only); virus-free diluent with inhibitors was
207 prepared in parallel. In experiments using only L2 cells (Figures 1 and 4), the medium
208 was aspirated and cold inoculum was added on ice; in parallel, one well per treatment
209 was inoculated with virus-free diluent containing inhibitors to provide a background
210 value (none of the drugs affected this value throughout the experiments). The inoculated
211 cells were incubated at 4°C for 1 h, washed once with cold PBS, and re-fed with cold
212 medium containing the inhibitors; the plates were then moved to a 37°C incubator (t = 0).
213 For post-infection treatment, the medium was aspirated and replaced with warm medium

containing DMSO or inhibitor(s) at t = 1 h (Figures 1 and 4). At t = 7–8 h, the medium was aspirated, the cells were washed once with PBS, Glo Lysis buffer (Promega E2661) was added at 100 µL/well, and the plates were stored at −80°C prior to analysis. For analysis, the plates were warmed to room temperature, 100 µL/well of Steady-Glo reagent (Promega E2510) was added to the lysates, and the total luminescence was measured using a BioTek Synergy HT instrument. The experiments in Figure 5 comparing L2, 17Cl1, and DBT cells were performed similarly with the following modifications. Post-inoculation, all cells were immediately incubated at 37°C (t = 0). Cells were washed with warm PBS and re-fed with warm medium containing inhibitors at t = 1 h, removed from the incubator and allowed to equilibrate to room temperature at t = 7 h, and analyzed for luciferase activity at t = 7.5 h by adding 100 µL/well of Steady-Glo reagent directly to the culture medium and measuring the activity within 30 min; in parallel, separate plates were treated, mock-infected, and re-fed with medium containing inhibitors and assessed for cell viability by adding 100 uL/well of reconstituted CellTiter-Glo® reagent (Promega G7571) directly to the culture medium and proceeding according to the manufacturer's instructions. No post-infection treatment only condition was included in the viability assays. The HEK-293T experiments in Figure 2 and Figure 7 were performed similarly to the L2/DBT/17Cl1 cell experiments with the following modifications. HEK-293T cells were re-seeded into 96-well plates at 5×10^4 cells/well on day 1 post-transfection and infected on day 2 post-transfection. All cells were infected at MOI = 0.05 pfu/cell and luciferase activity was assessed 7.5 hpi. The EGFP reporter experiments (Figure 8) were performed similarly to Figures 1 and 4 with the following modifications: the pre-infection treatment cells were washed and re-fed with medium

containing DMSO alone at t = 1 h, and the post-infection treatment condition cells were treated with DMSO alone during pre-treatment and infection and washed and re-fed with medium containing inhibitors beginning at t = 1 h. At t = 10 h, the cells were washed once with PBS, lysed with Reporter Lysis Buffer (Promega E3971), and frozen at -80°C to complete lysis; after thawing, the EGFP fluorescence endpoint was read with a BioTek Synergy HT plate reader (485/20 nm excitation filter, 528/20 nm emission filter, gain = 120). In all experiments, the final DMSO concentration was the same across all treatments and is indicated in the figure legend for each experiment.

tmprss2 mRNA measurement. Confluent wells of cells in 6-well plates were harvested and mRNA purified using TRIzol™ reagent (Thermo Fisher Scientific) according to the manufacturer's instructions with the following modifications: a second chloroform extraction (1:1 v/v) was performed on the aqueous phase and an ethanol precipitation step was added after the isopropanol precipitation. Kidney and prostate from 7–8-week-old male C57Bl/6 mice were homogenized in TRIzol™ and RNA purified similarly. RNA was diluted to 200 ng/uL and treated using the TURBO DNA-*free*™ kit (Thermo Fisher Scientific) to remove residual genomic DNA. Mouse universal reference total RNA (BD Biosciences S3296) was used as an additional control. cDNA was prepared from 350 ng of DNA-free RNA per 20-µL reaction using Superscript® III reverse transcriptase (Thermo Fisher Scientific) according to the manufacturer's instructions. The amounts of *Actb* and *Tmprss2* cDNA were assessed using quantitative PCR with iQ™ SYBR® Green SuperMix (Bio-Rad) with 2 uL cDNA per 25-uL reaction; the organ cDNA was diluted 1:5 prior to qPCR. The *Tmprss2* primers spanned the junction of exons 12 and 13

(F: 5′-ACAACAACCTAATCACACCAGCCAT-3′; R: 5′-AGCCACCAGATCCCATTCTTCAAAG-3′).

Immunoblotting. L2 cells were seeded at 2.5×10^5 cells/well and HEK-293T cells were seeded 1 dpt at 3.5×10^5 cells/well in 24-well plates and infected the next day (2 dpt for the HEK-293T cells) with the indicated virus diluted in DMEM with 2% FBS (t = 0 hpi). The cells were incubated at 37°C for 1 h and rocked by hand every 15 minutes, washed 3× (L2 cells) or 1× (HEK-293T cells) with warm PBS, and re-fed with fresh medium. For the L2 cells, the medium was removed at 5 hpi and replaced with medium containing the indicated treatment with a final DMSO concentration of 1%. At 16 hpi (L2 cells) or 18 hpi (HEK-293T cells), the cells were washed once with PBS and lysed with 1% NP-40 alternative (EMD Millipore 492018) in PBS with EDTA-free protease inhibitor cocktail (Roche 11836170001) plus 2 mM EDTA. Lysates were centrifuged at 700 × *g* at 4°C for 10 min to pellet the nuclei, and the post-nuclear supernatants were used immediately or stored at −80°C. The total protein concentration in the lysates was checked using a BCA protein assay kit (Pierce 23225) and differed minimally among samples in all cases, so loading of equal total protein or equal volume of lysate was used interchangeably. Lysates were run on NuPAGE 3–8% Tris-acetate gels (Invitrogen) using the manufacturer-recommended reagents and the proteins transferred to PVDF membranes. Membranes were blocked for 30 min at room temperature or overnight at 4°C in Tris-buffered saline with 0.1% Tween-20 (TBST) with 10% nonfat dry milk (hereafter "block"), incubated with primary antibody (polyclonal goat anti-S AO4, a kind gift from K.V. Holmes, 1:1000 in block; monoclonal mouse anti-S2 5B19.2 (45) 1:1000 in block; monoclonal mouse anti-N clone 1-16-1, from J.L. Leibowitz, 1:1000 in block;

282 monoclonal mouse anti-CEACAM1 CC1 (46) 1:1000 in block; or polyclonal rabbit anti-
283 FLAG, Sigma F7425, 1:1000 in TBST) for 1 h at room temperature or overnight at 4°C,
284 washed 20 min with block and 2 × 10 min with TBST, incubated 30 min with species-
285 specific horseradish peroxidase-conjugated secondary antibody in block (rabbit anti-goat
286 IgG, Invitrogen 61-1620, 1:5000; goat anti-mouse IgG, Pierce 31430, 1:5000; or donkey
287 anti-rabbit IgG, GE NA934V, 1:10,000), developed with Western Lightning or Western
288 Lightning Plus enhanced chemiluminescence reagent (Perkin Elmer), and imaged using
289 an Amersham Imager 600 (GE). For detection of additional substrates, membranes were
290 stripped 2 × 10 min with mild stripping buffer (1.5% glycine, 0.1% sodium dodecyl
291 sulfate, 1% Tween 20, pH 2.2) and washed twice with PBS and twice with TBST before
292 blocking and re-probing. Horseradish peroxidase-conjugated anti-β-tubulin (Abcam
293 21058) was used as a loading control and was diluted 1:1000 in TBST and hybridized for
294 1 h at room temperature, followed by washing and detection as described for conjugated
295 secondary antibodies.
296 *Syncytia formation assay.* L2 cells (100% confluent) or HEK-293β5 cells on dpt 2 (~80%
297 confluent) in 24-well plates were infected with the indicated EGFP-expressing virus at an
298 MOI of 0.01 (L2) or 0.1 (HEK-293β5) pfu/cell. The cells were incubated for 1 h at 37°C
299 and rocked at 15 min intervals, then washed with PBS and re-fed with L2 medium or
300 HEK-293T medium (t = 0). Five hours post-infection (L2) or 1 h post-infection (HEK-
301 293β5), the medium was replaced by medium containing DMSO or the indicated
302 inhibitor(s) at the indicated concentration(s) (final DMSO concentration of 1% for L2
303 cells and 0.1% for HEK-293β5 cells). At 16 hpi (L2) or 18 hpi (HEK-293β5), the cells
304 were washed once with PBS, fixed for 20 min with 4% paraformaldehyde in PBS, and

washed 3 × 5 min with PBS. Fluorescence was detected using a Nikon Eclipse TE2000-U fluorescence microscope with a 488 nm excitation filter.

RESULTS

JHM.SD is relatively resistant to bafilomycin A. We first used the luciferase reporter viruses to determine whether JHM.SD and A59 differed in sensitivity to inhibitors of endosomal proteases. Bafilomycin A inhibits the endosomal H^+-ATPase and thereby indirectly inhibits acid-activated endosomal proteases such as cathepsins (47). The assay was performed in L2 cells, an MHV-susceptible cell line previously used to compare the effect of bafilomycin A between A59 and MHV-2 (4). As entry of cell-associated MHV has been observed >1 h after washing (48), the treatment was maintained throughout the infection (Figure 1, top), and the effects of bafilomycin on late infection events were assessed separately by infecting untreated cells in parallel and beginning treatment at 1 hpi, after which bafilomycin A was previously shown to have minimal effect on MHV-2 infection of L2 cells (4) (Figure 1, middle). As post-entry treatment significantly affected A59 infection, the effect of the pre-infection treatment was divided by the effect of the post-infection treatment to correct for any post-entry effects (Figure 1, bottom). After correction, pre-treatment with bafilomycin A significantly decreased both JHM.SD and A59 infection at both doses. The effect did not differ significantly between the 10 nM and 100 nM doses for either virus but was significantly smaller for JHM.SD than for A59 at both doses. These results suggest that JHM.SD can use acid-dependent endosomal entry for infection of L2 cells but also exploits an acidification-independent entry route that is less available to A59.

328

329 **TMPRSS2 expression increases JHM.SD infection.** We next considered whether
330 acidification-independent JHM.SD infection might involve the cell surface serine
331 protease TMPRSS2, as has been shown for other coronaviruses. To address this
332 possibility, we co-transfected HEK-293T cells with MHV receptor (murine *Ceacam1a*-
333 4L) and increasing amounts of human *TMPRSS2* (h*TMPRSS2*) to generate receptor-
334 bearing cells that also expressed TMRPSS2 protein. We found that TMPRSS2 expression
335 increased JHM.SD infection but not A59 infection (Figure 2A): both the amount of
336 TMPRSS2 transfected and the virus strain had statistically significant and interactive
337 effects on luciferase activity, whereas transfection with a catalytically inactive mutant of
338 TMPRSS2 had minimal effect (data not shown). Treatment with the surface serine
339 protease inhibitor camostat beginning 3 h before infection abolished the effect of
340 TMPRSS2 on JHM.SD infection (Figure 2B), demonstrating that camostat inhibits
341 TMPRSS2 as expected and also suggesting that TMPRSS2 activity is required near the
342 time of infection. TMPRSS2 also increased JHM.SD infection in the presence of
343 bafilomycin A (Figure 2C), indicating that the effect of TMPRSS2 does not depend on
344 endosomal acidification. Finally, TMPRSS2 transfection did increase A59 infection in
345 the presence of bafilomycin A (Figure 2D), indicating that TMPRSS2-dependent
346 infection is available to A59 when the acidification-dependent pathway is blocked. Taken
347 together, these results show that TMPRSS2 activity can promote MHV infection:
348 specifically, TMPRSS2 increases JHM.SD infection of untreated cells and both JHM.SD
349 and A59 infection of bafilomycin A-treated cells.

TMPRSS2 overexpression decreases productive MHV infection and syncytia formation. We next investigated whether TMPRSS2 cleaves the JHM S spike and whether it cleaves the viral receptor CEACAM1a, as reported for the SARS-CoV receptor ACE2. We first co-transfected HEK-293T cells with m*Ceacam1a* and h*TMPRSS2* and examined protein size and expression by immunoblotting. CEACAM1a appeared as a doublet, with a major band consistent with the 110-kDa size of the full-length glycoprotein and a slower-migrating minor band sometimes visible in highly concentrated CEACAM1 preparations, especially protein purified from mouse intestinal brush border membranes (49, 50). Increasing expression of TMPRSS2 eliminated the upper band and ultimately decreased the strength of the major CEACAM1a band; however, no new species consistent with cell-associated TMPRSS2-cleaved CEACAM1a was seen in either uninfected or A59-infected cells (Figure 3A, top). These changes seemed most consistent with either shedding of CEACAM1a from the cell surface or suppression of CEACAM1a expression. As soluble receptor generally neutralizes MHV (51) and has been shown to induce S1/S2 dissociation of JHM S and thus compromise infectivity (52), we did not attribute the effect of TMPRSS2 expression on infection to shedding of soluble CEACAM1a by TMPRSS2. Wild-type TMPRSS2 was difficult to detect in cell lysates, although the active-site mutant TMPRSS2-S441A was well expressed (Figure 3A, bottom), consistent with reports of autocatalysis and subsequent shedding of the peripheral (C-terminal) TMPRSS2 fragment (53). We next infected co-transfected HEK-293T cells but found that expression of m*Ceacam1a* from the high-level expression vector pCAGGS severely limited expression of viral proteins and release of infectious virus (data not shown); therefore, m*Ceacam1a* was expressed from a

373 constitutive low-level expression vector using the thymidine kinase promoter (pTK) in
374 this and all further experiments in which late post-infection events (>8 hpi) were
375 examined in human cell lines. Under these conditions, transfection with pCAGGS-
376 h*TMPRSS2*-FLAG, which had promoted JHM.SD entry (Figure 2), actually decreased
377 productive MHV infection. Increasing expression of active TMPRSS2 decreased the
378 levels of the viral structural proteins S and N in cells infected with JHM.SD, A59, or a
379 chimeric virus bearing the MHV-2 spike (rA59/S_{MHV-2}) that is entirely cathepsin-
380 dependent for entry (Figure 3B). However, the polyclonal anti-S antibody AO4
381 recognized a possible TMPRSS2 S2′ product (expected size 60–80 kD (8, 26, 27)) only
382 for MHV-2 S. Immunoblotting with the monoclonal anti-S antibody 5B19.2, which
383 recognizes JHM.SD and A59 S and has been mapped to the MHV fusion peptide,
384 revealed an approximately 150-kD species of S that increased in density with increasing
385 TMPRSS2 expression (Figure 3C). This size is inconsistent with S2′ cleavage and may
386 indicate cleavage C-terminal to the fusion peptide, which would be expected to inactivate
387 S for fusion. Furthermore, increasing expression of TMPRSS2 significantly decreased
388 release of infectious virus for JHM.SD, rA59, and rA59/SMHV-2 (Figure 3D). Finally,
389 expression of active TMPRSS2 actually decreased syncytia formation by a chimeric virus
390 bearing the JHM.SD spike (rA59/$S_{JHM.SD}$-EGFP); the effect was blocked by the serine
391 protease inhibitor camostat, confirming that the decrease in cell-cell fusion was due to
392 TMPRSS2 activity (Figure 3E). Taken together, these results indicate that the level of
393 TMPRSS2 overexpression that promoted JHM.SD entry in Figure 3 is detrimental to
394 productive infection; the loss of both cell-associated CEACAM1a and viral protein
395 expression may indicate that this level of TMPRSS2 activity is cytotoxic. Co-expression

396 of MHV S and TMPRSS2 did result in new S cleavage products, but these cleavages may
397 not represent S2′ cleavage and did not promote cell-cell fusion. We concluded that we
398 could not further elucidate the role of TMPRSS2 in MHV infection using this
399 overexpression system.
400 **MHV infection is sensitive to metalloprotease inhibition.** Given the difficulty of
401 interpreting results from cells overexpressing TMPRSS2, we sought to augment our
402 findings in TMPRSS2-expressing HEK-293T cells by examining the role of endogenous
403 mouse TMPRSS-family proteases in MHV-permissive cell lines. We first examined
404 m*Tmprss2* mRNA expression by RT-qPCR but found that the m*Tmprss2* mRNA levels in
405 MHV target cells were at or below the limit of detection; Table 1 shows the results from
406 the only experiment in three attempts in which we consistently detected mtmprss2 in L2
407 cells. A single preliminary experiment using primary mouse cells yielded similar results,
408 with very low levels of m*Tmprss2* mRNA in neurons and astrocytes and none detected in
409 microglia or macrophages (data not shown). We concluded that endogenous TMPRSS2 is
410 unlikely to contribute to MHV infection in these target cells. We next investigated
411 whether another member of the TMPRSS family might facilitate JHM.SD infection of L2
412 cells by treating L2 cells with the surface serine protease inhibitor camostat, which is
413 expected to inhibit all 20 TMPRSS family members. As in Figure 1, cells were pre-
414 treated with protease inhibitors with and without bafilomycin (Figure 4, top panel), and
415 the results were normalized to those from cells treated post-entry (Figure 4, middle and
416 bottom panels). Camostat only slightly decreased JHM.SD infection: the significant 31%
417 reduction in Figure 4 was the strongest effect observed in 3 independent experiments, and
418 the effect did not reach significance in one of those experiments. We therefore tested a

variety of other protease inhibitors: the non-cell-penetrating cysteine protease inhibitor E64, the non-cell-penetrating aspartyl protease inhibitor pepstatin A, and the metalloprotease inhibitor batimastat. Batimastat strongly decreased infection by both JHM.SD and A59 even after correction for the substantial post-entry effect (Figure 4); most strikingly, combined treatment with batimastat and bafilomycin A completely inhibited infection by both viruses. Therefore, MHV infection of L2 cells appears to involve a batimastat-sensitive metalloprotease.

To ensure that the effect of batimastat was due to metalloprotease inhibition, we next employed another hydroxamate metalloprotease inhibitor, TAPI-1. Batimastat and TAPI-1 were applied to three MHV-susceptible cell lines and their effects on cell viability and JHM.SD infection assessed. In all three cell lines, both drugs were essentially non-toxic (Fig. 5A) and significantly decreased JHM.SD infection; in L2 and DBT cells, both drugs also further decreased infection when combined with bafilomycin A (Fig. 5B). The effects of the inhibitors varied in magnitude among the cell types (Fig. 5C): infection of 17Cl1 cells decreased greatly in response to bafilomycin A, accounting for 85% of the total variation (2-way ANOVA), but only slightly in response to metalloprotease inhibitors (7.7% of total variation), whereas infection of DBT cells decreased markedly in response to metalloprotease inhibitors (83% of total variation) but actually increased slightly in response to bafilomycin A alone. We did not observe the complete inhibition of infection by combined bafilomycin A/metalloprotease inhibitor treatment seen in Fig. 4, which we attribute to differences in the infection procedure (synchronization was omitted because 17Cl1 cells did not tolerate washing after incubation at 4°C). Together, these results indicate that metalloprotease inhibition

442 decreases MHV infection in multiple cell types and that the decrease in reporter gene
443 expression is not due to cytotoxicity. As MHV does not encode a viral metalloprotease,
444 the most logical conclusion is that a cell surface metalloprotease contributes to MHV
445 entry.

446 **Metalloprotease inhibitors reduce MHV-mediated syncytia formation without**
447 **blocking S1/S2 cleavage.** Addition of batimastat 1 h post-infection strongly decreased
448 luciferase reporter activity (Fig. 4) with minimal evidence of cytotoxicity (Fig. 5). As
449 MHV-induced cell-cell fusion begins only shortly after detectable viral protein
450 expression, we hypothesized that batimastat might inhibit MHV S-induced cell-cell
451 fusion. We therefore examined the effects of protease inhibitors on syncytia formation
452 and MHV spike cleavage in cells infected with isogenic EGFP-expressing MHV strains
453 bearing the syncytia-forming JHM.SD or A59 spike or the non-syncytia-forming MHV-2
454 spike. In parallel, we treated cells with camostat to determine whether TMPRSS-family
455 proteases contributed to cell-cell fusion. As S1/S2 cleavage is a prerequisite for MHV-
456 mediated cell-cell fusion, we also employed furin inhibitor I as a positive control for
457 inhibition of S1/S2 cleavage and syncytia formation. Addition of batimastat 5 h post-
458 infection substantially decreased syncytia formation by rA59/$S_{JHM.SD}$-EGFP and rA59-
459 EGFP (Figure 6A); the effect of batimastat was even greater than that of furin inhibitor I,
460 while camostat had no apparent effect. Immunoblotting of infected cell lysates showed
461 that both batimastat and furin inhibitor I reduced the levels of JHM.SD and A59 S but not
462 MHV-2 S protein, consistent with a loss of JHM.SD and A59 expansion through syncytia
463 formation.

464 S1/S2 cleavage is associated with MHV syncytia formation (4, 54), but the 110-
465 kDa S1/S2 cleavage products were still detected in batimastat-treated cells, indicating
466 that batimastat does not inhibit cell-cell fusion by blocking S1/S2 cleavage.
467 Unfortunately, inhibition of S2′ cleavage could not be assessed because no bands
468 consistent with S2′ were visible in the control samples, as in Figure 3. In contrast, furin
469 inhibitor I greatly decreased S1/S2 cleavage of the A59 spike (Figure 6B) but did not
470 completely inhibit cell-cell fusion (Figure 6A); surprisingly, it did not completely inhibit
471 cleavage of the JHM.SD spike even at the relatively high concentration of 100 μM
472 (Figure 6B), suggesting that the JHM.SD S1/S2 site is either exceptionally susceptible to
473 furin cleavage or cleavable by other cellular proteases. These results indicate that MHV-
474 mediated cell-cell fusion relies on a batimastat-sensitive metalloprotease that is not
475 required for cleavage at S1/S2.
476 **TMPRSS2 restores infection but not cell-cell fusion in the presence of**
477 **metalloprotease inhibition**. We next investigated whether metalloprotease and
478 TMPRSS2 are redundant for MHV infection by treating h*TMPRSS*2-transfected cells
479 with batimastat, bafilomycin A, or both inhibitors. Both batimastat and bafilomycin A
480 decreased JHM.SD infection in HEK-293 cells, as in mouse cells. TMPRSS2 expression
481 significantly increased infection in a dose-dependent manner under all conditions (Fig.
482 7A). The ability of TMPRSS2 to replace metalloprotease activity in cell-to-cell fusion
483 was difficult to assess because TMPRSS2 overexpression itself decreases syncytia size
484 (Fig. 3E): the overwhelming majority of infection foci in tmprss2-transfected cells were
485 unicellular regardless of treatment (Figure 7B). We therefore conclude that TMPRSS2
486 can replace metalloprotease activity for MHV entry but not for cell-cell fusion.

The MHV-2 spike protein is resistant to metalloprotease inhibition during entry. Finally, we sought to link the effect of metalloprotease inhibition to cleavage of MHV S during entry. We reasoned that if the metalloprotease cleaves MHV S to activate it for fusion, then infection by the MHV-2 spike, being entirely dependent on cathepsin B and/or L activity, should be resistant to metalloprotease inhibitors. To test this hypothesis, L2 cells were pretreated with batimastat and/or bafilomycin A and infected at 4°C (as in Figures 1 and 4) with the isogenic chimeric viruses rA59-EGFP, rA59/$S_{JHM.SD}$-EGFP, and rA59/S_{MHV-2}-EGFP. To separate the effects of metalloprotease inhibition on entry and cell-cell fusion, both inhibitors were removed at 1 hpi and replaced with medium containing DMSO only ("pre" treatments); in parallel, infected cells pretreated with DMSO alone were treated with inhibitors beginning at 1 hpi ("post" treatments); the DMSO control cells were treated with fresh medium containing DMSO at each time point. Consistent with previous results (4) and our hypothesis, rA59/S_{MHV-2}-EGFP entry was highly sensitive to bafilomycin A but resistant to batimastat treatment (Figure 8). All three viruses were essentially blocked by combined treatment with bafilomycin A and batimastat, as seen in Figure 4, and the effects of post-infection treatment were also S-dependent, as in Figure 6. These strain-dependent effects strongly suggest that batimastat inhibits a metalloprotease that interacts with the viral S protein, and the pronounced suppression of JHM.SD and A59 by batimastat treatment from -3 to 1 hpi demonstrates that the drug inhibits MHV entry.

DISCUSSION

Coronaviruses use diverse proteases for entry at different cellular sites, including acid-dependent endosomal/lysosomal proteases such as cathepsins to enter cells via the

late endosome (4, 8, 10-14, 18, 55), furin to enter via the early endosome (48, 56), and TMPRSS2 to enter presumably at or near the cell surface (13, 15-18, 57). Among MHV strains, MHV-2 depends on the endosomal cysteine proteases cathepsin B and L, while A59 can be blocked by combined inhibition of cysteine and aspartyl lysosomal proteases (4, 48). This study extends the analysis of MHV protease use to include the brain-adapted JHM.SD strain of MHV, which mediates cell-cell fusion independent of the receptor protein, and cell-surface serine proteases such as TMPRSS2. We found that bafilomycin A (an inhibitor of endosomal acidification and therefore indirectly of acid-dependent endosomal proteases) only modestly decreased entry and overexpression of TMPRSS2 greatly enhanced entry of JHM.SD relative to their effects on strain A59. However, inhibition of endogenous surface serine protease activity had only a modest effect on JHM.SD infection; instead, an as-yet unidentified batimastat-sensitive metalloprotease appeared to be most important for both viral entry and virus-mediated cell-cell fusion. The list of proteases that may mediate coronavirus fusion must therefore be expanded to include metalloproteases. The contribution of metalloprotease activity to JHM.SD infection varied widely among the tested cell lines, suggesting that either the level of MHV-promoting metalloprotease activity or the efficiency of the endosomal entry pathway differs between cell types. We also observed MHV strain-dependent effects of bafilomycin A and batimastat on viruses bearing the MHV-2, A59, and JHM.SD spike proteins. Together, these results suggest that metalloprotease use could underlie the spike-dependent neurovirulence of JHM.SD (32, 33).

Batimastat and TAPI-1, the metalloprotease inhibitors used in the present study, are broad-spectrum inhibitors of two metalloprotease families: the matrix

metalloproteases (MEROPS family M10; abbreviated MMP) and the *A-D*isintegrin-*A*nd-*M*etalloprotease group (MEROPS family M12; abbreviated ADAM or ADAMTS) (58). One member of these families, ADAM17, was previously shown to mediate uptake of SARS-CoV S-pseudotyped particles but not productive infection (23, 28-30); otherwise, these proteases have not to the best of our knowledge been implicated in viral entry. In the mouse, these families comprise some 69 catalytically active proteases (58-60); we are currently working to identify the specific metalloprotease(s) involved in MHV infection.

Many studies of protease use in coronavirus fusion have employed exogenous expression of cellular proteases or addition of recombinant soluble proteases. The results we obtained from overexpression of TMRPSS2 suggest that such experiments should be interpreted with caution: although TMPRSS2 increased JHM.SD entry, the level of overexpression used was detrimental to virus production and cell-cell fusion. We judged the potential for confounding effects to be significant and did not attempt to determine whether the loss of CEACAM1a and MHV protein in cell lysates was due to shedding, loss of MHV amplification by cell-to-cell spread, or general cytotoxicity. It remains unclear whether endogenous expression of any TMPRSS protease in any cell type promotes JHM.SD entry without decreasing overall virus yield, as would be necessary for JHM.SD to have evolved to use these proteases for CNS infection. We therefore conclude that enhancement of JHM.SD infection by TMPRSS2 suggests that this virus is susceptible to fusion activation by non-endosomal proteases, but we cannot infer a role for TMPRSS2 in MHV infection of the CNS from the results of the present study.

Our findings pose three apparent discrepancies with published results that must be addressed. First, A59 was previously shown to be largely insensitive to inhibition of

557 endosomal acidification (4). However, in that case the inhibition was removed shortly
558 after infection and the infection measured as the viral titer at 16 hpi. A59 can enter
559 asynchronously (48), and it seems likely that some A59 infection occurred after the
560 removal of the inhibitor or that robust second-round infection compensated for entry
561 inhibition during inoculation. More recently, the presence of a post-fusion A59 S2
562 cleavage fragment was not affected by the metalloprotease inhibitor phosphoramidon
563 (26); however, phosphoramidon does not inhibit batimastat-sensitive MMPs and ADAM
564 proteases (58, 60). Finally, JHM.SD infection was previously reported to resist inhibition
565 by endosomotropic weak bases (37), which indirectly inhibit cathepsins similarly to
566 bafilomycin A; however, that study was performed in DBT cells, in which we observed
567 increased JHM.SD infection after bafilomycin A treatment (Figure 5). Therefore, we
568 consider the results of the current study to be consistent with the published literature.
569 Given that the coronavirus S2 domain requires proteolysis for fusion activation
570 (8), that the metalloprotease inhibitor acts early in infection and also blocks cell-cell
571 fusion, and that the effect varies among MHV S proteins, the simplest interpretation of
572 our findings is that a metalloprotease cleaves some MHV S proteins to activate S2 for
573 fusion. Collectively, the results of the present study and other studies of coronavirus entry
574 suggest that there are parallel acid-dependent (i.e., late endosomal/lysosomal)-dependent
575 and acid-independent (i.e., surface or early endosomal metalloprotease or TMPRSS2)-
576 dependent pathways for MHV entry (Figure 9A). In this model, JHM.SD cannot
577 efficiently access the acid-dependent pathway and relies on the acid-independent
578 pathway, making it less sensitive to bafilomycin A and more sensitive to metalloprotease
579 inhibition and TMPRSS2 overexpression. By contrast, A59 enters efficiently via the acid-

dependent pathway but is less efficiently cleaved by acid-independent proteases, making it more susceptible to bafilomycin A and less susceptible to TMPRSS2 expression or metalloprotease inhibition, while MHV-2 is blocked by bafilomycin A alone and is relatively resistant to metalloprotease inhibition. Simultaneous blockade of both pathways by combined bafilomycin A/batimastat treatment therefore abrogates infection by all strains. The mechanism underlying these inter-strain differences is less clear; we suspect that the instability of JHM.SD S inactivates many potentially infectious particles due to S1/S2 dissociation and/or premature fusion triggering during endosomal uptake and/or acidification, whereas the more stable A59 and MHV-2 spike proteins survive until appropriately activated by endosomal proteases. Metalloprotease or TMPRSS2 cleavage would thus rescue JHM.SD infection by allowing virions to enter the acid-independent pathway (up to 90% or more of the total inoculum, judging by the >10-fold enhancement of infection by TMPRSS2 in HEK-293T cells in Figure 2). Such parallel fusion protein processing could greatly expand the cell and organ tropism of MHV.

Although our findings seem most consistent with parallel entry pathways (Figure 9A), we cannot rule out a sequential cleavage model in which all MHV ultimately enters via endosomal protease cleavage but prior cleavage by surface proteases greatly increases the efficiency of endosomal protease cleavage (Figure 9B). Assuming that endosomal proteases retain some activity in face of high-concentration bafilomycin A treatment, we can hypothesize that the native JHM.SD spike is poorly cleaved by acid-dependent proteases (creating dependence on acid-independent proteases) but is readily cleaved and thus primed by acid-independent proteases (decreasing the effect of bafilomycin A by making the residual endosomal protease activity more effective), while the A59 spike is a

603 better substrate for endosomal proteases in the absence of prior cleavage (making it less
604 dependent on acid-independent protease activity) but also less efficiently primed
605 (rendering it more susceptible to bafilomycin A). In this case, MHV-2 might be
606 unaffected by metalloprotease cleavage because S1/S2 cleavage is required to expose the
607 metalloprotease site. This model could even be invoked to explain the effect of batimastat
608 on cell-cell fusion, as some paramyxovirus fusion proteins have been shown to require
609 secretion, internalization, cathepsin cleavage, and recycling to the plasma membrane for
610 activation (reviewed in (61)). The idea of multiple proteolytic cleavage sites in S2 is not
611 unprecedented — at least two groups have now reported heterogeneous coronavirus S
612 post-entry cleavage products suggestive of cleavage at multiple sites within S2 (26, 27),
613 consistent with the idea that S2 is cleaved by more than one protease during virus-cell
614 fusion — but which of these cleavages are fusion-activating, which prime the protein for
615 a definitive fusion-activating cleavage, and which are simply destructive remains to be
616 clarified.

617 In conclusion, MHV strains JHM.SD and A59 exhibit strain-specific dependence
618 on endosomal acidification and acid-independent proteases, including a previously
619 unsuspected batimastat-sensitive metalloprotease, for infection. These results hint that
620 cleavage of MHV spike by different proteases either provides alternative entry pathways
621 or greatly facilitates a definitive fusion-activating event. MHV strains differ markedly in
622 organ and tissue tropism in a spike-dependent manner despite the use of a common
623 receptor; the current study joins other recent work in suggesting that the availability of
624 specific fusion-activating proteases may greatly influence coronavirus virulence.
625

626 **FUNDING INFORMATION**

627 This work was supported by NIH grants R01AI600210 to SRW and K08AI098503 to

628 JMP.

629

630 **REFERENCES**
631
632 1. Bertram S, Glowacka I, Steffen I, Kuhl A, Pohlmann S. Novel insights into
633 proteolytic cleavage of influenza virus hemagglutinin. Rev Med Virol. 2010;20(5):298-
634 310. doi: 10.1002/rmv.657. PubMed PMID: 20629046.
635 2. Zhou Y, Vedantham P, Lu K, Agudelo J, Carrion R, Jr., Nunneley JW, Barnard
636 D, Pohlmann S, McKerrow JH, Renslo AR, Simmons G. Protease inhibitors targeting
637 coronavirus and filovirus entry. Antiviral Res. 2015;116:76-84. doi:
638 10.1016/j.antiviral.2015.01.011. PubMed PMID: 25666761.
639 3. Heald-Sargent T, Gallagher T. Ready, set, fuse! The coronavirus spike protein
640 and acquisition of fusion competence. Viruses. 2012;4(4):557-80. doi:
641 10.3390/v4040557. PubMed PMID: 22590686; PubMed Central PMCID: PMC3347323.
642 4. Qiu Z, Hingley ST, Simmons G, Yu C, Das Sarma J, Bates P, Weiss SR.
643 Endosomal proteolysis by cathepsins is necessary for murine coronavirus mouse hepatitis
644 virus type 2 spike-mediated entry. J Virol. 2006;80(12):5768-76. doi:
645 10.1128/JVI.00442-06. PubMed PMID: 16731916; PubMed Central PMCID:
646 PMC1472567.
647 5. Yamada YK, Takimoto K, Yabe M, Taguchi F. Acquired fusion activity of a
648 murine coronavirus MHV-2 variant with mutations in the proteolytic cleavage site and
649 the signal sequence of the S protein. Virology. 1997;227(1):215-9. doi:
650 10.1006/viro.1996.8313. PubMed PMID: 9007076.
651 6. Gombold JL, Hingley ST, Weiss SR. Fusion-defective mutants of mouse hepatitis
652 virus A59 contain a mutation in the spike protein cleavage signal. J Virol.
653 1993;67(8):4504-12. PubMed PMID: 8392595; PubMed Central PMCID: PMC237834.
654 7. de Haan CA, Stadler K, Godeke GJ, Bosch BJ, Rottier PJ. Cleavage inhibition of
655 the murine coronavirus spike protein by a furin-like enzyme affects cell-cell but not
656 virus-cell fusion. J Virol. 2004;78(11):6048-54. doi: 10.1128/JVI.78.11.6048-6054.2004.
657 PubMed PMID: 15141003; PubMed Central PMCID: PMC415802.
658 8. Belouzard S, Chu VC, Whittaker GR. Activation of the SARS coronavirus spike
659 protein via sequential proteolytic cleavage at two distinct sites. Proc Natl Acad Sci U S
660 A. 2009;106(14):5871-6. doi: 10.1073/pnas.0809524106. PubMed PMID: 19321428;
661 PubMed Central PMCID: PMC2660061.
662 9. Belouzard S, Millet JK, Licitra BN, Whittaker GR. Mechanisms of coronavirus
663 cell entry mediated by the viral spike protein. Viruses. 2012;4(6):1011-33. doi:
664 10.3390/v4061011. PubMed PMID: 22816037; PubMed Central PMCID: PMC3397359.
665 10. Simmons G, Gosalia DN, Rennekamp AJ, Reeves JD, Diamond SL, Bates P.
666 Inhibitors of cathepsin L prevent severe acute respiratory syndrome coronavirus entry.
667 Proc Natl Acad Sci U S A. 2005;102(33):11876-81. doi: 10.1073/pnas.0505577102.
668 PubMed PMID: 16081529; PubMed Central PMCID: PMC1188015.
669 11. Huang IC, Bosch BJ, Li F, Li W, Lee KH, Ghiran S, Vasilieva N, Dermody TS,
670 Harrison SC, Dormitzer PR, Farzan M, Rottier PJ, Choe H. SARS coronavirus, but not
671 human coronavirus NL63, utilizes cathepsin L to infect ACE2-expressing cells. J Biol
672 Chem. 2006;281(6):3198-203. doi: 10.1074/jbc.M508381200. PubMed PMID:
673 16339146.
674 12. Qian Z, Dominguez SR, Holmes KV. Role of the spike glycoprotein of human
675 Middle East respiratory syndrome coronavirus (MERS-CoV) in virus entry and syncytia

formation. PLoS One. 2013;8(10):e76469. doi: 10.1371/journal.pone.0076469. PubMed PMID: 24098509; PubMed Central PMCID: PMC3789674.

13. Gierer S, Bertram S, Kaup F, Wrensch F, Heurich A, Kramer-Kuhl A, Welsch K, Winkler M, Meyer B, Drosten C, Dittmer U, von Hahn T, Simmons G, Hofmann H, Pohlmann S. The spike protein of the emerging betacoronavirus EMC uses a novel coronavirus receptor for entry, can be activated by TMPRSS2, and is targeted by neutralizing antibodies. J Virol. 2013;87(10):5502-11. doi: 10.1128/JVI.00128-13. PubMed PMID: 23468491; PubMed Central PMCID: PMC3648152.

14. Regan AD, Shraybman R, Cohen RD, Whittaker GR. Differential role for low pH and cathepsin-mediated cleavage of the viral spike protein during entry of serotype II feline coronaviruses. Vet Microbiol. 2008;132(3-4):235-48. doi: 10.1016/j.vetmic.2008.05.019. PubMed PMID: 18606506; PubMed Central PMCID: PMC2588466.

15. Matsuyama S, Nagata N, Shirato K, Kawase M, Takeda M, Taguchi F. Efficient activation of the severe acute respiratory syndrome coronavirus spike protein by the transmembrane protease TMPRSS2. J Virol. 2010;84(24):12658-64. doi: 10.1128/JVI.01542-10. PubMed PMID: 20926566; PubMed Central PMCID: PMC3004351.

16. Shulla A, Heald-Sargent T, Subramanya G, Zhao J, Perlman S, Gallagher T. A transmembrane serine protease is linked to the severe acute respiratory syndrome coronavirus receptor and activates virus entry. J Virol. 2011;85(2):873-82. doi: 10.1128/JVI.02062-10. PubMed PMID: 21068237; PubMed Central PMCID: PMC3020023.

17. Glowacka I, Bertram S, Muller MA, Allen P, Soilleux E, Pfefferle S, Steffen I, Tsegaye TS, He Y, Gnirss K, Niemeyer D, Schneider H, Drosten C, Pohlmann S. Evidence that TMPRSS2 activates the severe acute respiratory syndrome coronavirus spike protein for membrane fusion and reduces viral control by the humoral immune response. J Virol. 2011;85(9):4122-34. doi: 10.1128/JVI.02232-10. PubMed PMID: 21325420; PubMed Central PMCID: PMC3126222.

18. Kawase M, Shirato K, van der Hoek L, Taguchi F, Matsuyama S. Simultaneous treatment of human bronchial epithelial cells with serine and cysteine protease inhibitors prevents severe acute respiratory syndrome coronavirus entry. J Virol. 2012;86(12):6537-45. doi: 10.1128/JVI.00094-12. PubMed PMID: 22496216; PubMed Central PMCID: PMC3393535.

19. Shirato K, Kanou K, Kawase M, Matsuyama S. Clinical Isolates of Human Coronavirus 229E Bypass the Endosome for Cell Entry. J Virol. 2016. doi: 10.1128/JVI.01387-16. PubMed PMID: 27733646.

20. Shirato K, Matsuyama S, Ujike M, Taguchi F. Role of proteases in the release of porcine epidemic diarrhea virus from infected cells. J Virol. 2011;85(15):7872-80. doi: 10.1128/JVI.00464-11. PubMed PMID: 21613395; PubMed Central PMCID: PMC3147927.

21. Chaipan C, Kobasa D, Bertram S, Glowacka I, Steffen I, Tsegaye TS, Takeda M, Bugge TH, Kim S, Park Y, Marzi A, Pohlmann S. Proteolytic activation of the 1918 influenza virus hemagglutinin. J Virol. 2009;83(7):3200-11. doi: 10.1128/JVI.02205-08. PubMed PMID: 19158246; PubMed Central PMCID: PMC2655587.

22. Bottcher E, Matrosovich T, Beyerle M, Klenk HD, Garten W, Matrosovich M. Proteolytic activation of influenza viruses by serine proteases TMPRSS2 and HAT from human airway epithelium. J Virol. 2006;80(19):9896-8. doi: 10.1128/JVI.01118-06. PubMed PMID: 16973594; PubMed Central PMCID: PMC1617224.
23. Heurich A, Hofmann-Winkler H, Gierer S, Liepold T, Jahn O, Pohlmann S. TMPRSS2 and ADAM17 cleave ACE2 differentially and only proteolysis by TMPRSS2 augments entry driven by the severe acute respiratory syndrome coronavirus spike protein. J Virol. 2014;88(2):1293-307. doi: 10.1128/JVI.02202-13. PubMed PMID: 24227843; PubMed Central PMCID: PMC3911672.
24. Matsuyama S, Ujike M, Morikawa S, Tashiro M, Taguchi F. Protease-mediated enhancement of severe acute respiratory syndrome coronavirus infection. Proc Natl Acad Sci U S A. 2005;102(35):12543-7. doi: 10.1073/pnas.0503203102. PubMed PMID: 16116101; PubMed Central PMCID: PMCPMC1194915.
25. Belouzard S, Madu I, Whittaker GR. Elastase-mediated activation of the severe acute respiratory syndrome coronavirus spike protein at discrete sites within the S2 domain. J Biol Chem. 2010;285(30):22758-63. doi: 10.1074/jbc.M110.103275. PubMed PMID: 20507992; PubMed Central PMCID: PMCPMC2906266.
26. Wicht O, Burkard C, de Haan CA, van Kuppeveld FJ, Rottier PJ, Bosch BJ. Identification and characterization of a proteolytically primed form of the murine coronavirus spike proteins after fusion with the target cell. J Virol. 2014;88(9):4943-52. doi: 10.1128/JVI.03451-13. PubMed PMID: 24554652; PubMed Central PMCID: PMCPMC3993802.
27. Millet JK, Whittaker GR. Host cell entry of Middle East respiratory syndrome coronavirus after two-step, furin-mediated activation of the spike protein. Proc Natl Acad Sci U S A. 2014;111(42):15214-9. doi: 10.1073/pnas.1407087111. PubMed PMID: 25288733; PubMed Central PMCID: PMC4210292.
28. Haga S, Nagata N, Okamura T, Yamamoto N, Sata T, Yamamoto N, Sasazuki T, Ishizaka Y. TACE antagonists blocking ACE2 shedding caused by the spike protein of SARS-CoV are candidate antiviral compounds. Antiviral Res. 2010;85(3):551-5. doi: 10.1016/j.antiviral.2009.12.001. PubMed PMID: 19995578.
29. Haga S, Yamamoto N, Nakai-Murakami C, Osawa Y, Tokunaga K, Sata T, Yamamoto N, Sasazuki T, Ishizaka Y. Modulation of TNF-alpha-converting enzyme by the spike protein of SARS-CoV and ACE2 induces TNF-alpha production and facilitates viral entry. Proc Natl Acad Sci U S A. 2008;105(22):7809-14. doi: 10.1073/pnas.0711241105. PubMed PMID: 18490652; PubMed Central PMCID: PMC2409424.
30. Glowacka I, Bertram S, Herzog P, Pfefferle S, Steffen I, Muench MO, Simmons G, Hofmann H, Kuri T, Weber F, Eichler J, Drosten C, Pohlmann S. Differential downregulation of ACE2 by the spike proteins of severe acute respiratory syndrome coronavirus and human coronavirus NL63. J Virol. 2010;84(2):1198-205. doi: 10.1128/JVI.01248-09. PubMed PMID: 19864379; PubMed Central PMCID: PMC2798380.
31. Park JE, Li K, Barlan A, Fehr AR, Perlman S, McCray PB, Jr., Gallagher T. Proteolytic processing of Middle East respiratory syndrome coronavirus spikes expands virus tropism. Proc Natl Acad Sci U S A. 2016;113(43):12262-7. doi: 10.1073/pnas.1608147113. PubMed PMID: 27791014.

32. Phillips JJ, Chua MM, Lavi E, Weiss SR. Pathogenesis of chimeric MHV4/MHV-A59 recombinant viruses: the murine coronavirus spike protein is a major determinant of neurovirulence. J Virol. 1999;73(9):7752-60. PubMed PMID: 10438865; PubMed Central PMCID: PMC104302.
33. Phillips JJ, Chua MM, Rall GF, Weiss SR. Murine coronavirus spike glycoprotein mediates degree of viral spread, inflammation, and virus-induced immunopathology in the central nervous system. Virology. 2002;301(1):109-20. PubMed PMID: 12359451.
34. Gallagher TM, Buchmeier MJ, Perlman S. Cell receptor-independent infection by a neurotropic murine coronavirus. Virology. 1992;191(1):517-22. PubMed PMID: 1413526.
35. Bender SJ, Phillips JM, Scott EP, Weiss SR. Murine coronavirus receptors are differentially expressed in the central nervous system and play virus strain-dependent roles in neuronal spread. J Virol. 2010;84(21):11030-44. doi: 10.1128/JVI.02688-09. PubMed PMID: 20739537; PubMed Central PMCID: PMC2953140.
36. Miura TA, Travanty EA, Oko L, Bielefeldt-Ohmann H, Weiss SR, Beauchemin N, Holmes KV. The spike glycoprotein of murine coronavirus MHV-JHM mediates receptor-independent infection and spread in the central nervous systems of Ceacam1a-/- Mice. J Virol. 2008;82(2):755-63. doi: 10.1128/JVI.01851-07. PubMed PMID: 18003729; PubMed Central PMCID: PMC2224565.
37. Gallagher TM, Escarmis C, Buchmeier MJ. Alteration of the pH dependence of coronavirus-induced cell fusion: effect of mutations in the spike glycoprotein. J Virol. 1991;65(4):1916-28. PubMed PMID: 1848311; PubMed Central PMCID: PMC240014.
38. Kuo L, Godeke GJ, Raamsman MJ, Masters PS, Rottier PJ. Retargeting of coronavirus by substitution of the spike glycoprotein ectodomain: crossing the host cell species barrier. J Virol. 2000;74(3):1393-406. PubMed PMID: 10627550; PubMed Central PMCID: PMC111474.
39. Masters PS, Rottier PJ. Coronavirus reverse genetics by targeted RNA recombination. Curr Top Microbiol Immunol. 2005;287:133-59. PubMed PMID: 15609511.
40. de Haan CA, van Genne L, Stoop JN, Volders H, Rottier PJ. Coronaviruses as vectors: position dependence of foreign gene expression. J Virol. 2003;77(21):11312-23. PubMed PMID: 14557617; PubMed Central PMCID: PMCPMC229330.
41. Zhang R, Li Y, Cowley TJ, Steinbrenner AD, Phillips JM, Yount BL, Baric RS, Weiss SR. The nsp1, nsp13, and M proteins contribute to the hepatotropism of murine coronavirus JHM.WU. J Virol. 2015;89(7):3598-609. doi: 10.1128/JVI.03535-14. PubMed PMID: 25589656; PubMed Central PMCID: PMC4403414.
42. Das Sarma J, Fu L, Tsai JC, Weiss SR, Lavi E. Demyelination determinants map to the spike glycoprotein gene of coronavirus mouse hepatitis virus. J Virol. 2000;74(19):9206-13. PubMed PMID: 10982367; PubMed Central PMCID: PMC102119.
43. Das Sarma J, Scheen E, Seo SH, Koval M, Weiss SR. Enhanced green fluorescent protein expression may be used to monitor murine coronavirus spread in vitro and in the mouse central nervous system. J Neurovirol. 2002;8(5):381-91. doi: 10.1080/13550280260422686. PubMed PMID: 12402164.

Journal of Virology

44. Hingley ST, Gombold JL, Lavi E, Weiss SR. MHV-A59 fusion mutants are attenuated and display altered hepatotropism. Virology. 1994;200(1):1-10. doi: 10.1006/viro.1994.1156. PubMed PMID: 8128613.
45. Collins AR, Knobler RL, Powell H, Buchmeier MJ. Monoclonal antibodies to murine hepatitis virus-4 (strain JHM) define the viral glycoprotein responsible for attachment and cell--cell fusion. Virology. 1982;119(2):358-71. PubMed PMID: 6281979.
46. Holmes KV, Williams RK, Cardellichio CB, Compton SR, Stephensen CB, Snyder SW, Frana MF, Jiang GS, Smith A, Knobler RL. Is the 110K glycoprotein the only receptor for MHV and does its expression determine species specificity? Adv Exp Med Biol. 1990;276:37-44. PubMed PMID: 1966425.
47. Oda K, Nishimura Y, Ikehara Y, Kato K. Bafilomycin A1 inhibits the targeting of lysosomal acid hydrolases in cultured hepatocytes. Biochem Biophys Res Commun. 1991;178(1):369-77. PubMed PMID: 2069575.
48. Burkard C, Verheije MH, Wicht O, van Kasteren SI, van Kuppeveld FJ, Haagmans BL, Pelkmans L, Rottier PJ, Bosch BJ, de Haan CA. Coronavirus Cell Entry Occurs through the Endo-/Lysosomal Pathway in a Proteolysis-Dependent Manner. PLoS Pathog. 2014;10(11):e1004502. doi: 10.1371/journal.ppat.1004502. PubMed PMID: 25375324; PubMed Central PMCID: PMC4223067.
49. Williams RK, Jiang GS, Snyder SW, Frana MF, Holmes KV. Purification of the 110-kilodalton glycoprotein receptor for mouse hepatitis virus (MHV)-A59 from mouse liver and identification of a nonfunctional, homologous protein in MHV-resistant SJL/J mice. J Virol. 1990;64(8):3817-23. PubMed PMID: 2164599; PubMed Central PMCID: PMCPMC249677.
50. Pensiero MN, Dveksler GS, Cardellichio CB, Jiang GS, Elia PE, Dieffenbach CW, Holmes KV. Binding of the coronavirus mouse hepatitis virus A59 to its receptor expressed from a recombinant vaccinia virus depends on posttranslational processing of the receptor glycoprotein. J Virol. 1992;66(7):4028-39. PubMed PMID: 1318394; PubMed Central PMCID: PMCPMC241205.
51. Zelus BD, Wessner DR, Dveksler GS, Holmes KV. Neutralization of MHV-A59 by soluble recombinant receptor glycoproteins. Adv Exp Med Biol. 1998;440:3-9. PubMed PMID: 9782258.
52. Gallagher TM. A role for naturally occurring variation of the murine coronavirus spike protein in stabilizing association with the cellular receptor. J Virol. 1997;71(4):3129-37. PubMed PMID: 9060676; PubMed Central PMCID: PMCPMC191445.
53. Afar DE, Vivanco I, Hubert RS, Kuo J, Chen E, Saffran DC, Raitano AB, Jakobovits A. Catalytic cleavage of the androgen-regulated TMPRSS2 protease results in its secretion by prostate and prostate cancer epithelia. Cancer Res. 2001;61(4):1686-92. PubMed PMID: 11245484.
54. Hingley ST, Leparc-Goffart I, Seo SH, Tsai JC, Weiss SR. The virulence of mouse hepatitis virus strain A59 is not dependent on efficient spike protein cleavage and cell-to-cell fusion. J Neurovirol. 2002;8(5):400-10. doi: 10.1080/13550280260422703. PubMed PMID: 12402166.
55. Simmons G, Bertram S, Glowacka I, Steffen I, Chaipan C, Agudelo J, Lu K, Rennekamp AJ, Hofmann H, Bates P, Pohlmann S. Different host cell proteases activate

the SARS-coronavirus spike-protein for cell-cell and virus-cell fusion. Virology. 2011;413(2):265-74. doi: 10.1016/j.virol.2011.02.020. PubMed PMID: 21435673; PubMed Central PMCID: PMC3086175.

56. Yamada Y, Liu DX. Proteolytic activation of the spike protein at a novel RRRR/S motif is implicated in furin-dependent entry, syncytium formation, and infectivity of coronavirus infectious bronchitis virus in cultured cells. J Virol. 2009;83(17):8744-58. doi: 10.1128/JVI.00613-09. PubMed PMID: 19553314; PubMed Central PMCID: PMC2738192.

57. Bertram S, Dijkman R, Habjan M, Heurich A, Gierer S, Glowacka I, Welsch K, Winkler M, Schneider H, Hofmann-Winkler H, Thiel V, Pohlmann S. TMPRSS2 activates the human coronavirus 229E for cathepsin-independent host cell entry and is expressed in viral target cells in the respiratory epithelium. J Virol. 2013;87(11):6150-60. doi: 10.1128/JVI.03372-12. PubMed PMID: 23536651; PubMed Central PMCID: PMC3648130.

58. Rawlings ND, Walter M, Barrett AJ, Bateman A. MEROPS: the database of proteolytic enzymes, their substrates and inhibitors. Nucleic Acids Res. 2014;42:D503-D9. Epub 2013 Oct 23. doi: 10.1093/nar/gkt953. PubMed PMID: 24157837; PubMed Central PMCID: PMC3964991.

59. The UniProt Consortium. Activities at the Universal Protein Resource (UniProt). Nucleic Acids Res. 2014;42:D191-D8. Epub 2013 Nov 18. doi: 10.1093/nar/gkt1140. PubMed PMID: 24253303; PubMed Central PMCID: PMC3965022.

60. Rawlings ND, Barrett AJ. MEROPS: the Peptidase Database [cited 2014 June 4]. Available from: http://merops.sanger.ac.uk.

61. Chang A, Dutch RE. Paramyxovirus fusion and entry: multiple paths to a common end. Viruses. 2012;4(4):613-36. doi: 10.3390/v4040613. PubMed PMID: 22590688; PubMed Central PMCID: PMC3347325.

sample	C_t (*Actb*)	C_t (*Tmprss2*)	C_t (*Tmprss2*) ≤ 40	ΔC_t
reference RNA	17.9	24.3	N/A	6.3
kidney	22.3	27.4	N/A	5.1
prostate	20.1	25.9	N/A	5.8
DBT	16.5 (0.3)	39.1 (1.1)	4/9*	22.6 (1.0)
17Cl1	16.0 (0.2)	38.3 (1.6)	6/9*	22.3 (1.5)
L2	16.3 (0.1)	33.5 (0.3)	9/9*	17.2 (0.3)

*C_t Values for cell lines are the mean and standard deviation of n = 3 cDNA samples prepared from separate wells of each cell type; each cDNA was then assayed in triplicate (9 reactions total). The final cycle number (40) was used for the *Tmprss2* C_t where no signal was otherwise detected. Data are representative of two independent experiments.

885

886 **Table 1: *TMPRSS2* mRNA expression in mouse cell lines.**

887

888 FIGURE LEGENDS

889 **Figure 1. JHM.SD is less sensitive than A59 to bafilomycin A.** Pretreated L2 cells
890 were infected with rJHM.SD-fluc or rA59-fluc at an approximate multiplicity of infection
891 (MOI) of 0.5 and then assayed for luciferase activity 7 hpi as described in the methods
892 section. In parallel, cells were infected and then treated with DMSO/bafilomycin A
893 beginning 1 h post-infection, and the pre-treatment effect (relative to DMSO alone for
894 each virus) was divided by the corresponding post-treatment effect to correct for post-
895 treatment effects. Top and middle: *: significant difference between the 0 and 10 nM or
896 100 nM treatment within each virus (2-way ANOVA with Dunnett's multiple
897 comparisons of simple effects within columns). Bottom: After correction, the effect of
898 bafilomycin A was significantly smaller for JHM.SD than for A59 (n = 5; 2-way
899 ANOVA: p = <0.0001 for the bafilomycin A effect, <0.0001 for the virus strain effect,
900 and 0.0008 for the interaction; *: significant difference (Tukey's multiple comparisons
901 between all cell means) within each MHV strain between the bafilomycin A treatment

and the 0 nM bafilomycin A control; #: significant difference between JHM.SD and A59 at the indicated bafilomycin A concentration (Tukey's multiple comparisons between all cell means). Data shown are representative of 3 independent experiments with n = 5 technical replicates.

Figure 2. TMPRSS2 activity directly mediates bafilomycin A-independent MHV infection. A. JHM.SD is more sensitive than A59 to TMPRSS2 transfection. HEK-293T cells co-transfected with pCAGGS-m*Ceacam1a*-4L and pCAGGS-h*TMPRSS2*-FLAG were infected with the indicated virus. Two-way ANOVA (n = 5): p = <0.0001 for the effects of TMPRSS2 and virus strain and their interaction; Tukey's multiple comparisons: * = the TMPRSS2 transfection levels at which the 2 viruses were significantly different from each other. B. Camostat abrogates the effect of TMPRSS2 on JHM.SD infection. Transfected HEK-293T cells were treated with DMSO or camostat (final DMSO concentration = 1.5%) prior to infection. Two-way ANOVA: p = <0.0001 for TMPRSS2 transfection, camostat treatment, and their interaction; Dunnett's multiple comparisons: # = significant difference from the no-TMPRSS2 control within the DMSO group (no significant difference from the no-TMPRSS2 control at any level of TMPRSS2 transfection within the camostat group). C. TMPRSS2 enhances JHM.SD infection in the presence of bafilomycin A. Transfected HEK-293T cells were treated with DMSO or bafilomycin A (final DMSO concentration = 0.5%) prior to infection with JHM.SD-fluc. Two-way ANOVA: p = <0.0001 for the effects of TMPRSS2 and bafilomycin A and their interaction; Dunnett's multiple comparisons test: # = significant difference from the no-TMPRSS2 control within the DMSO group and † = significant difference from the no-TMPRSS2 control within the bafilomycin A group. D. TMPRSS2 overcomes

926 bafilomycin A inhibition of A59 infection. Transfected HEK-293T cells were treated
927 with DMSO or bafilomycin A (final DMSO concentration = 0.5%) prior to infection with
928 rA59-fluc. Two-way ANOVA: p = <0.0001 for the effects of TMPRSS2 and bafilomycin
929 A and their interaction; Dunnett's multiple comparisons: # = the TMPRSS2 transfection
930 levels at which A59 infection differed from the no-TMPRSS2 control within the DMSO
931 group and † = the TMPRSS2 transfection levels at which A59 infection differed from the
932 no-TMPRSS2 control within the bafilomycin A group. All data are representative of at
933 least 2 independent experiments with n = 5 technical replicates.
934
935 **Figure 3. TMPRSS2 overexpression decreases productive MHV infection. A.**
936 TMPRSS2 decreases CEACAM1a protein. HEK-293T cells co-transfected with
937 pCAGGS-ceacam1a-4L and pCAGGS-h*TMPRSS2*-FLAG or pCAGGS-h*TMPRSS2*-
938 S441A-FLAG were infected with rA59/$S_{JHM.SD}$-EGFP and lysed for immunoblotting at
939 18 hpi. **B.** TMPRSS2 decreases cell-associated MHV protein. HEK-293T cells co-
940 transfected with pTK-m*Ceacam1a*-4L and pCAGGS-h*TMPRSS2*-FLAG or pCAGGS-
941 h*TMPRSS2*-S441A-FLAG were infected as indicated and lysed for immunoblotting 18
942 hpi. Goat polyclonal anti-S antibody AO4 was used to detect the S protein and mouse
943 anti-N mAb 1-16-1 to detect N protein. The vertical lines indicate boundaries between
944 non-adjacent lanes (rA59/$S_{JHM.SD}$-EGFP and rA59-EGFP were run on the same gel but
945 their positions were exchanged for consistency with other panels; rA59/S_{MHV-2}-EGFP and
946 the mock-infected cells were run in parallel on a separate gel). **C.** TMPRSS2 cleavage of
947 S may be nonproductive. Probing the lysates from (C) with anti-S2 mAb 5B19.2,
948 previously mapped to the fusion peptide, detected a ~150 kDa fragment (black box)

inconsistent with S2′ cleavage. **D.** TMPRSS2 decreases MHV titer. HEK-293T cells were co-transfected with pTK-m*Ceacam1a*-4L and pCAGGS-h*TMPRSS2*-FLAG or 200 ng of pCAGGS-h*TMPRSS2*-S441A-FLAG and infected with the indicated viruses; cell supernatants were collected at 18 hpi and titered. Both active and inactive TMPRSS2 significantly decreased the MHV titer (2-way ANOVA with Dunnett's multiple comparisons of each TMPRSS2 level with the 0 ng control within each virus; p = <0.0001 for the effect of the virus, <0.0001 for the effect of TMPRSS2 transfection, and 0.0045 for the interaction; *, $p < 0.05$; **, $p < 0.01$; ***, $p < 0.001$; ****, $p < 0.0001$ for the multiple comparisons). Data are representative of 2 independent experiments performed in triplicate. **E.** TMPRSS2 activity decreases syncytia size. HEK-293β5 cells were co-transfected with pTK-m*Ceacam1a*-4L and pCAGGS-h*TMPRSS2*-FLAG or pCAGGS-h*TMPRSS2*-S441A-FLAG and infected as in (B–D), treated at 2 hpi with DMSO or camostat as indicated (final DMSO concentration = 0.1% for all treatments), and fixed for microscopy at 18 hpi.

Figure 4. The metalloprotease inhibitor batimastat reduces JHM.SD and A59 infection of L2 cells. L2 cells were treated with DMSO or the indicated inhibitors as described in the Materials and Methods (1.5% DMSO final) and infected with rJHM.SD-fluc (left) or rA59-fluc (right), and luciferase activity was measured at 8 hpi. For each treatment, the effect of pretreatment relative to DMSO alone was divided by the effect of post-treatment relative to DMSO alone to correct for post-entry effects, and the results were analyzed using 2-way ANOVA with Dunnett's multiple comparisons tests comparing each protease inhibitor alone or with bafilomycin A to DMSO alone or with bafilomycin A, respectively. Both bafilomycin A and protease inhibitor treatment had

973 significant and interactive effects on both JHM.SD and A59 infection ($p < 0.0001$ for
974 protease inhibition, bafilomycin A, and the interaction for both JHM.SD and A59).
975 Asterisks indicate the level of significance of the results of Dunnett's multiple
976 comparisons tests of simple effects within columns (protease inhibitor vs. DMSO control
977 within each bafilomycin A treatment group; *, $p < 0.05$; **, $p < 0.01$; ***, $p < 0.001$;
978 ****, $p < 0.0001$). Data shown are representative of 3 independent experiments with n =
979 5 technical replicates.
980
981 **Figure 5. Cell-penetrating and extracellular metalloprotease inhibitors are non-toxic**
982 **and decrease JHM.SD infection in multiple cell lines.** Cells were pretreated with
983 batimastat or TAPI-1 and/or bafilomycin A (final DMSO concentration = 1.5% for all
984 treatments in all cells), infected with JHM.SD-fluc (A; MOI = 0.5) or mock-infected (B),
985 washed, and incubated for an additional 6 h at 37°C and 30 min at room temperature in
986 the presence of inhibitor before cell viability (A) and viral luciferase activity (B) were
987 assessed. Representative data from two independent experiments with n = 5 technical
988 replicates are shown. A: Both batimastat and TAPI-1 were essentially non-toxic under the
989 tested conditions. B: Both batimastat and TAPI-1 decreased infection in all cell types.
990 Asterisks show the result of two-way ANOVA with Dunnett's multiple comparisons test
991 of simple effects within columns (metalloprotease inhibitor vs. DMSO) for L2 and 17Cl1
992 cells and Tukey's multiple comparisons test between all cell means (not all results
993 shown) for DBT cells (*, $p < 0.05$; **, $p < 0.01$; ***, $p < 0.001$; ****, $p < 0.0001$). C:
994 Tabular results of two-way ANOVA on the data from panel B.
995

996 **Figure 6.** Batimastat inhibits syncytia formation but not S1/S2 cleavage. A. L2 cells were
997 infected (MOI = 0.01) as indicated. Five hours post-infection, the medium was replaced
998 with fresh medium containing the indicated inhibitor (final DMSO concentration = 1%).
999 Fifteen hours post-infection, the cells were fixed and infection analyzed by brightfield
1000 and fluorescence microscopy. B. L2 cells were infected (MOI = 0.1) as indicated. At 5
1001 hpi, the medium was replaced with fresh medium containing the indicated inhibitor. At
1002 16 hpi, the supernatant was removed and the cells lysed and subjected to immunoblotting
1003 with a polyclonal anti-S antibody (AO4). β-tubulin was detected as a loading control.
1004
1005 **Figure 7. TMPRSS2 is an alternative to metalloprotease for JHM.SD entry. A.**
1006 TMPRSS2 rescues blockade of JHM.SD entry by bafilomycin A, batimastat, or both.
1007 HEK-293T cells co-transfected with pTK-*mCeacam1a*-4L and pCAGGS-h*TMPRSS2*-
1008 FLAG were pre-treated with batimastat and/or bafilomycin A (final DMSO concentration
1009 = 1.5%) and infected with JHM.SD-fluc (MOI = 0.05 pfu/cell), and the treatment was
1010 maintained until the luciferase activity was assayed at 7.5 hpi. Two-way ANOVA (n = 5):
1011 p = <0.0001 for drug treatment, TMPRSS2 level, and the interaction between them; *:
1012 transfection levels at which Dunnett's multiple comparisons tests showed significant
1013 differences from baseline for all treatments. Data are representative of two independent
1014 experiments with n = 5 technical replicates. **B.** TMPRSS2 inefficiently rescues MHV
1015 cell-to-cell spread in the presence of batimastat. HEK-293β5 cells co-transfected with
1016 pTK-m*Ceacam1a*-4L and pCAGGS-htmprss2-FLAG or pCAGGS-h*TMPRSS2*-S441A-
1017 FLAG were infected with rA59/$S_{JHM.SD}$-EGFP (MOI = 0.1); at 2 hpi, the medium was
1018 replaced with medium containing DMSO, batimastat, camostat, or both, as indicated

(final DMSO concentration = 0.1% for all treatments), and syncytia formation was assessed at t = 18 h.

Figure 8. The effect of metalloprotease inhibition on MHV infection is S strain-specific. L2 cells were treated with batimastat (50 uM) and/or bafilomycin A (100 nM) or DMSO as described in the Materials and Methods (1.5% DMSO final for all conditions) and infected with isogenic chimeric viruses bearing the S protein from JHM.SD, A59, or MHV-2 (MOI = 0.5). Two-way ANOVA showed significant effects of treatment, strain, and interaction ($p < 0.0001$ for all); the asterisks represent the results of Tukey's multiple comparisons tests between each pair of viruses within each condition (level of significance for at least 2 of the 3 comparisons; *, $p < 0.05$; **, $p < 0.01$; ***, $p < 0.001$; ****, $p < 0.0001$). Data are representative of 2 independent experiments with n = 5 technical replicates.

Figure 9. Independent and sequential cleavage models of MHV entry. In the independent pathways model (A), JHM.SD is more efficiently cleaved by cell-surface acid-independent proteases (vertical stripes) such as metalloprotease or TMPRSS2 and fuses at the plasma membrane, whereas A59 better survives endocytosis and/or is more efficiently cleaved by acid-dependent endosomal proteases (horizontal stripes). In the sequential cleavage model (B), cleavage by acid-independent proteases produces a metastable intermediate that is more readily cleaved by endosomal proteases, and JHM.SD S is more efficiently cleaved by acid-independent proteases but less efficiently cleaved by endosomal proteases.

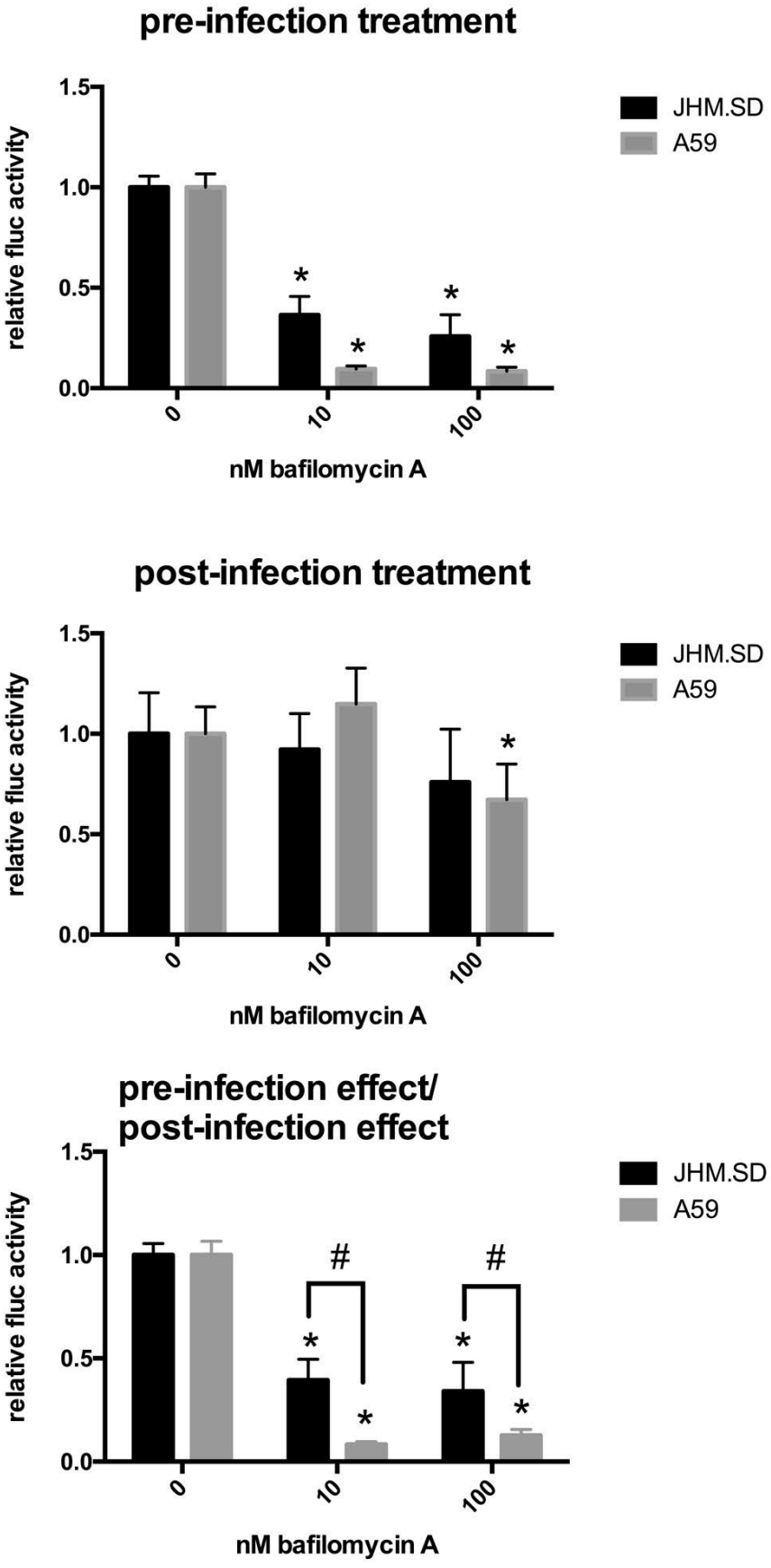

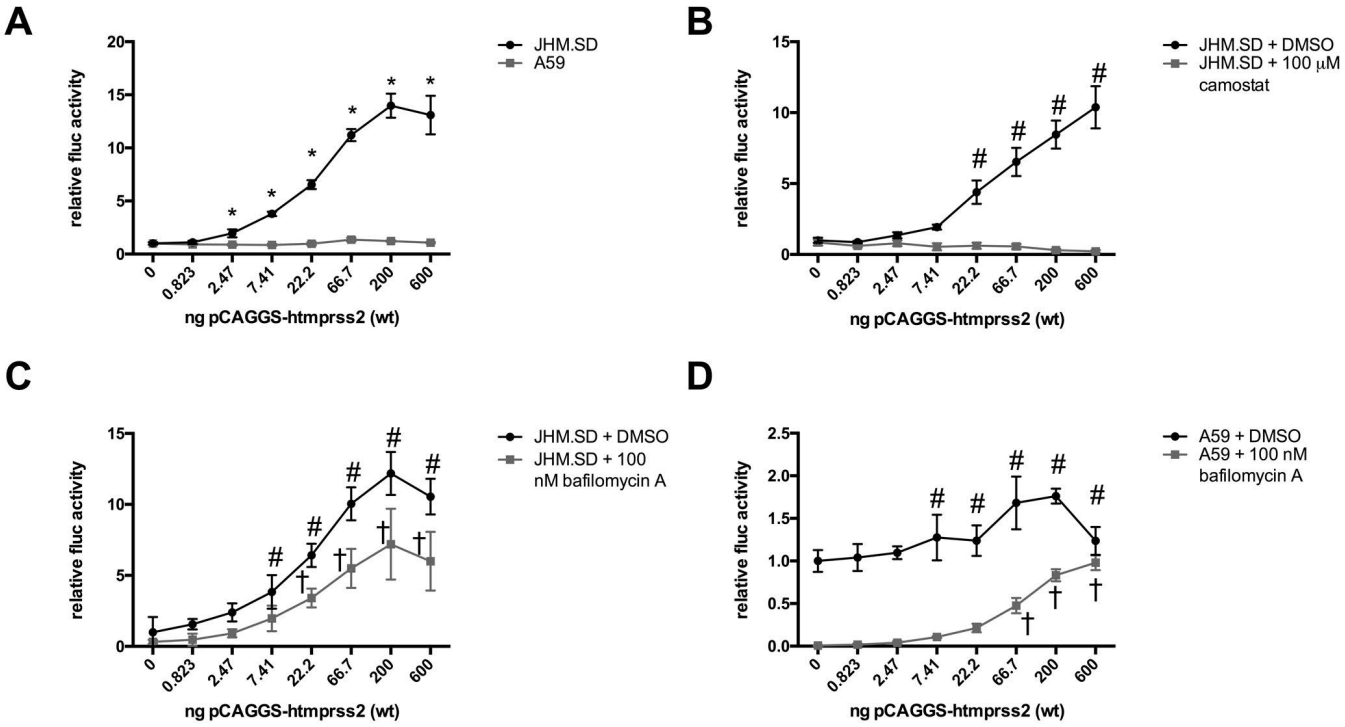

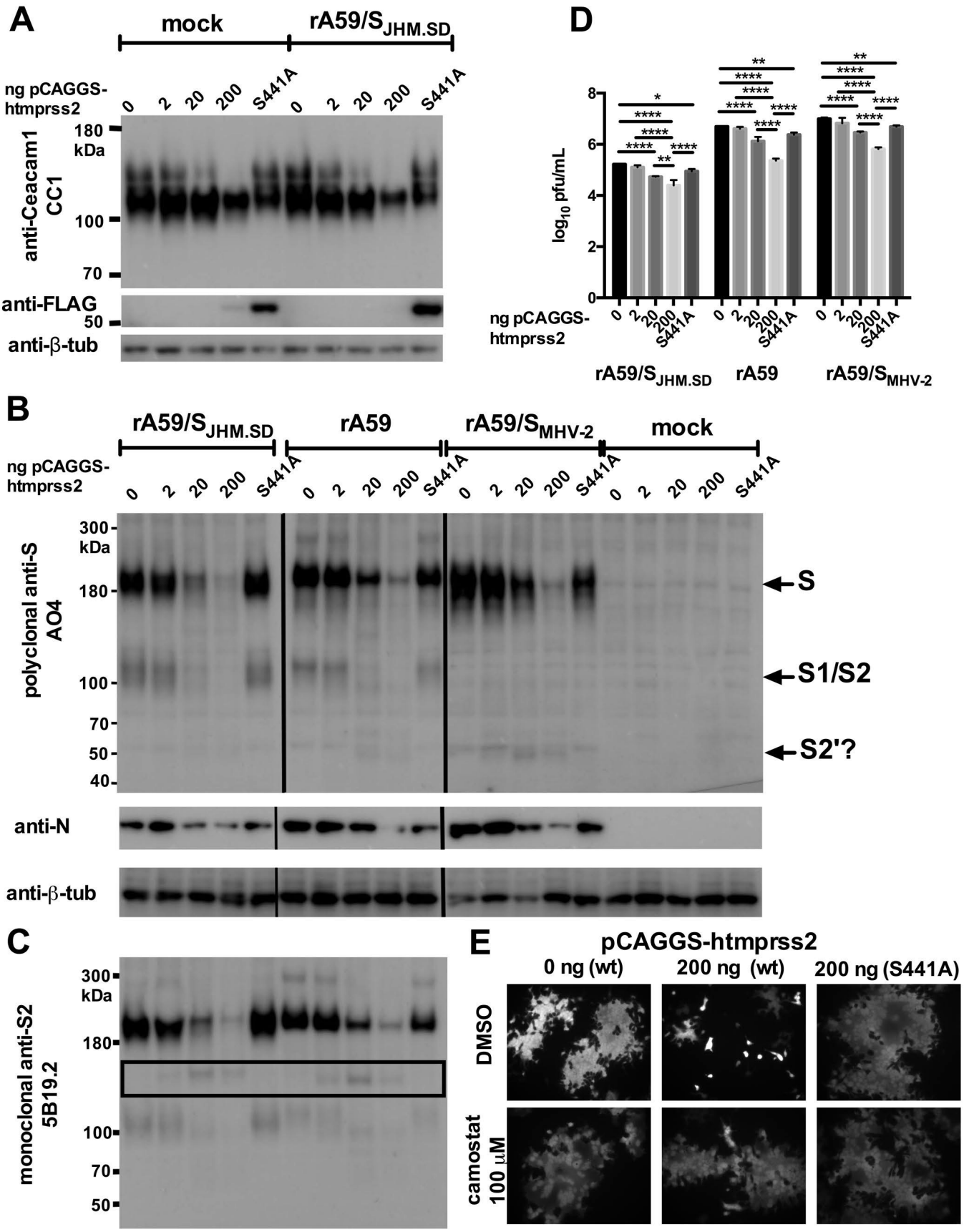

Journal of Virology

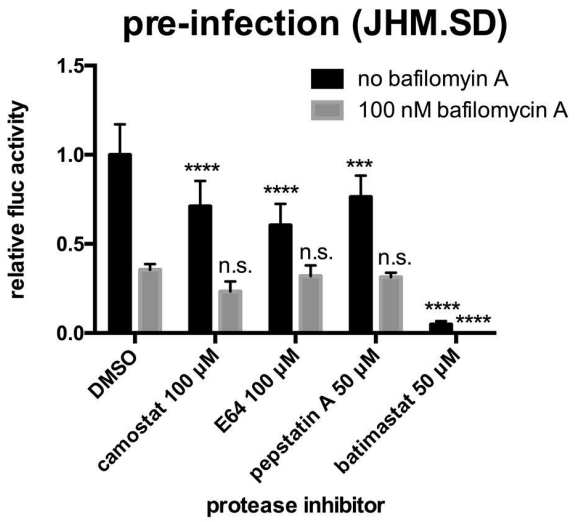

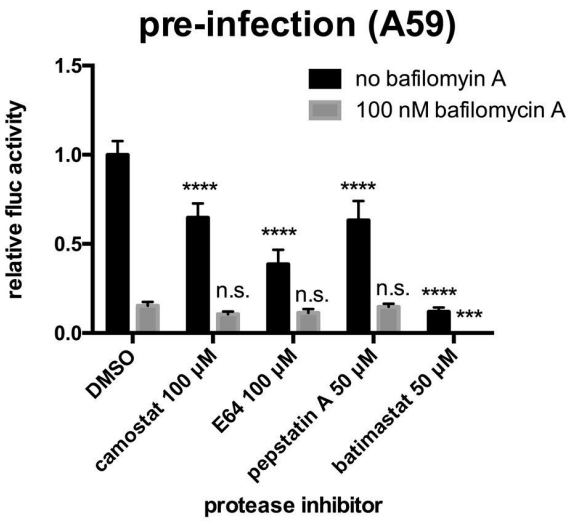

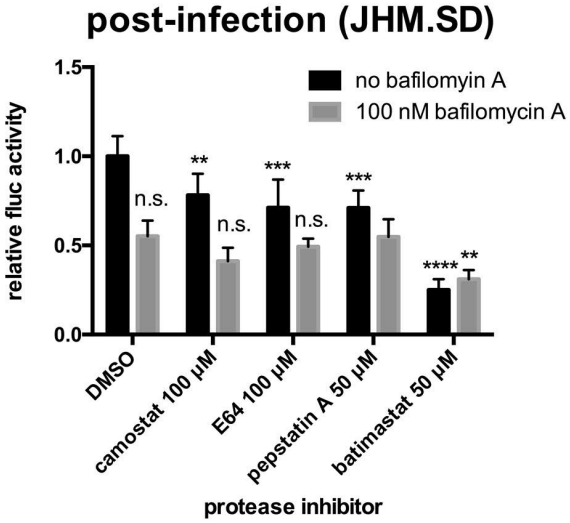

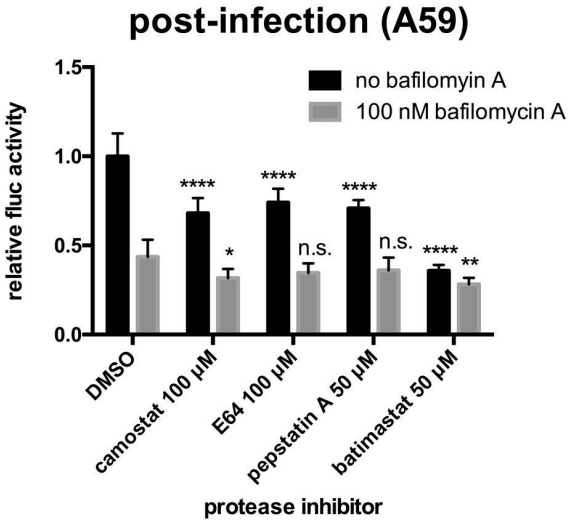

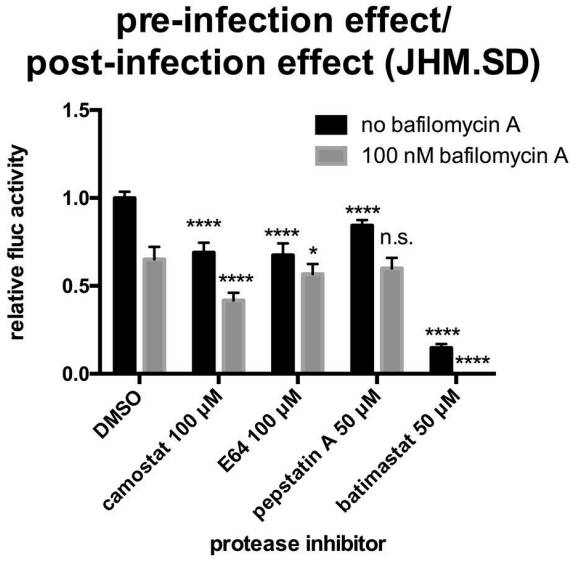

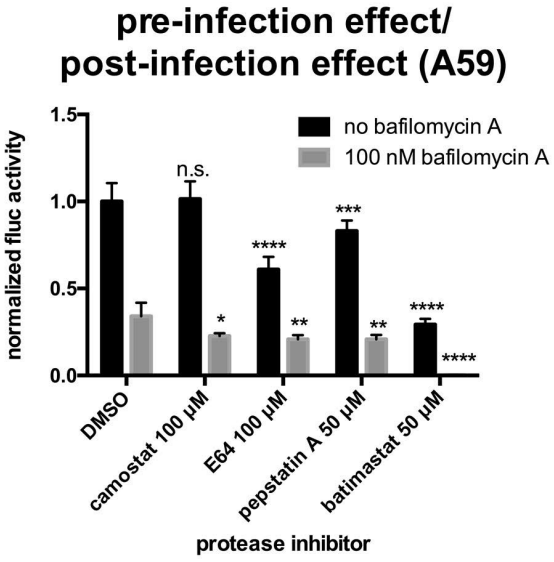

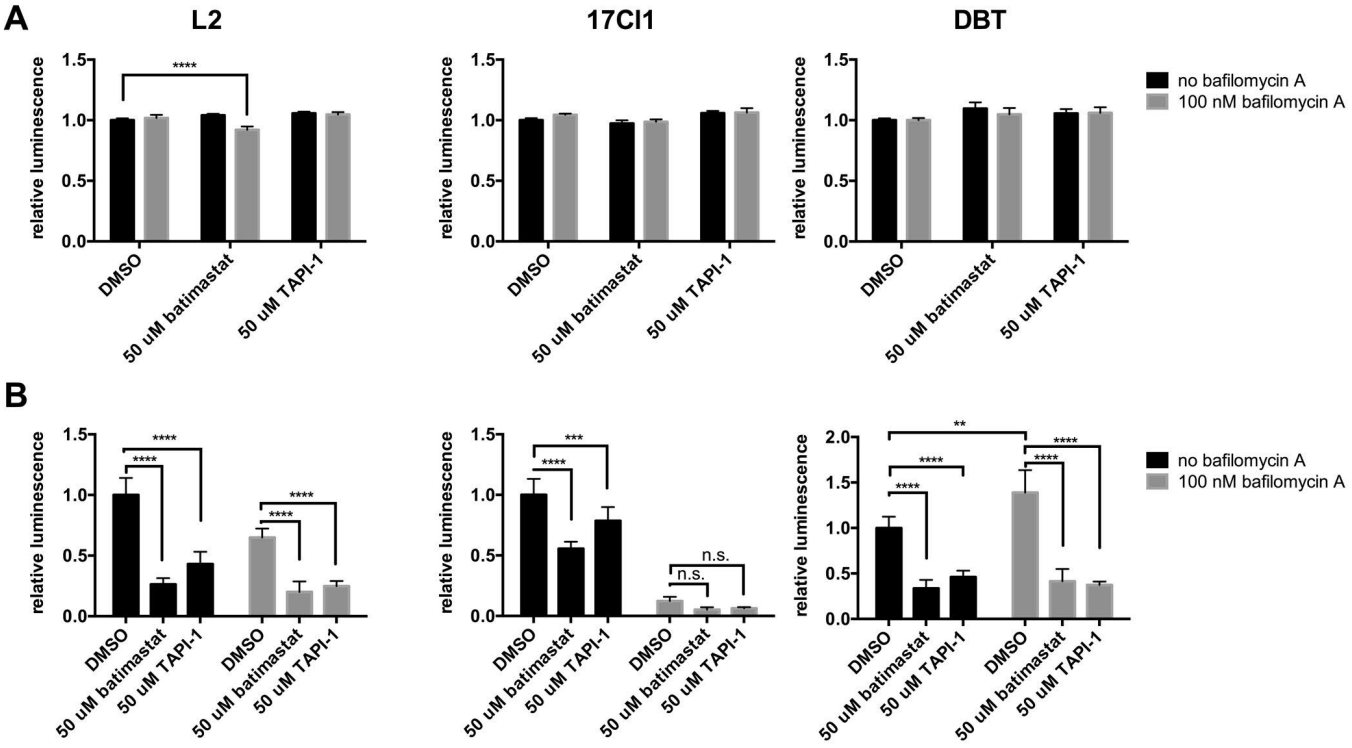

C

cell type	% of total variation: bafilomycin A	metalloprotease inhibitor	interaction
L2	11.46%****	77.18%****	4.05%**
17Cl1	84.96%****	7.69%****	4.07%****
DBT	2.37%*	83.34%****	5.68%**

Journal of Virology

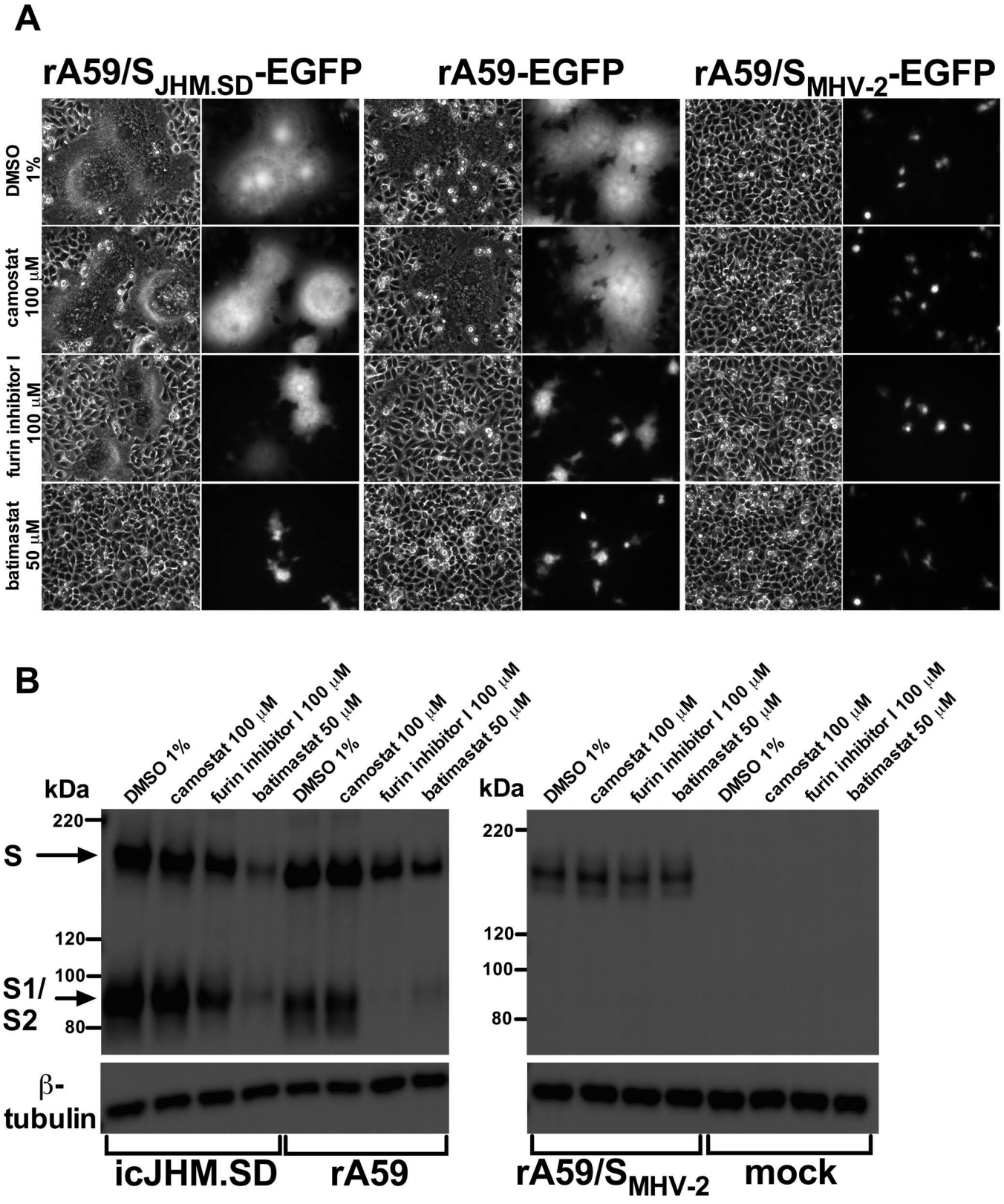

A

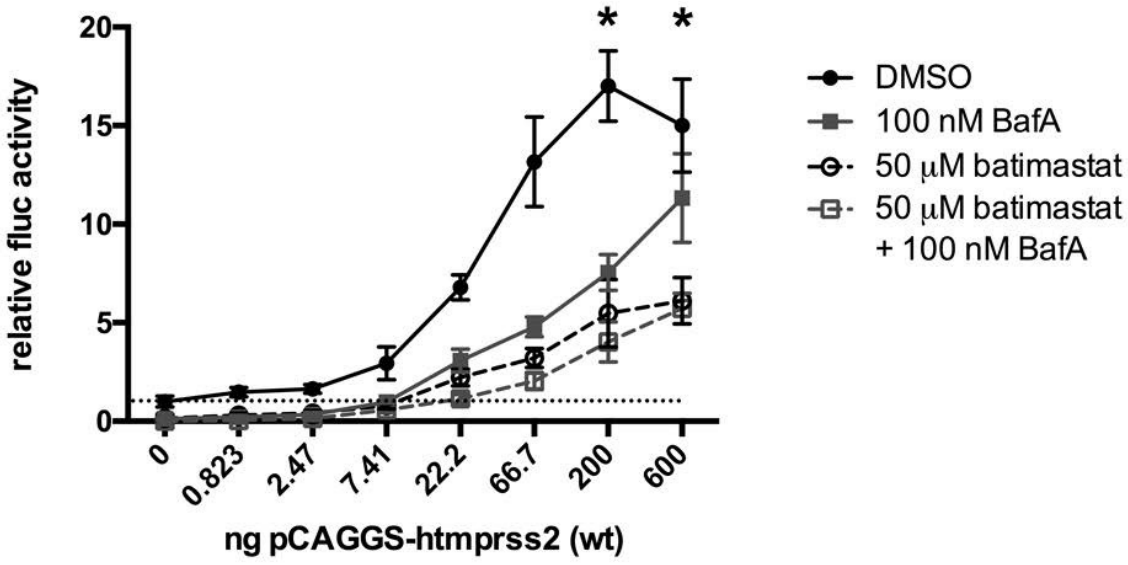

B